Egypt. J. Chem. **Vol. 67**, No. 5 pp. 285 - 305 (2024)

Egyptian Journal of Chemistry

http://ejchem.journals.ekb.eg/

Synthesis of some Sulfonamide Derivatives coupled with Salicylamide or Anisamide Scaffold as Potent PD-L1 Inhibitors and their Anti-proliferation Assay

Nagwa M. Abdelazeem[a], Mohammad Alwahsh[b], Alaaeldin M. F. Galal[c]*, Shahd Talhouni[b], Lama Hamadneh[d] and Atef G. Hanna [c]*

[a] *Organometallic and Organometalloid Chemistry Department, National Research Centre, Giza, Egypt*

[b] *Department of Pharmacy, Faculty of Pharmacy, Al-Zaytoonah University of Jordan, P.O. Box 130, Amman 11733, Jordan*

[c] *Chemistry of Natural Compounds Department, Pharmaceutical and Drug Industries Research Institute National Research Centre, 33 El Bohouth St. (former El Tahir St.), Dokki, Giza, 12622 Egypt.*

[d]*Department of Basic Medical Sciences, Faculty of Medicine, Al-Balqa Applied University. Al-Salt, Jordan*

Abstract

The present study explores the potential of the new sulfonamide derivatives coupled with salicylamide or anisamide scaffold as immune checkpoint PD-L1 inhibitors. Based on *in silico* virtual screening 32 derivatives were synthesized and tested in vitro as PD-L1 inhibitors using screening ELISA assay. Five compounds gave promising results with more than 50% inhibition. The most active, with activity 57.152%, was 5-Chloro-N-(4-(N-(3-fluorophenyl)sulfamoyl)phenethyl)salicylamide (**30**). The other compounds were 5-Chloro-2-methoxy-N-(4-(N-(4-fluorophenyl)sulfamoyl)benzyl)benzamide (**4**, 53.327%), 5-Chloro-2-methoxy-N-(4-(N-(4-methylphenyl)sulfamoyl)phenethyl)benzamide (**17**, 51.253%), 5-Chloro-N-(4-(N-(4-(trifluoromethyl) phenyl)sulfamoyl)phenethyl)salicylamide (**31**, 51.058%) and 5-Chloro-2-methoxy-N-(4-(N-(2,4-difluorophenyl)sulfamoyl) benzyl)benzamide (**7**, 50.993). The synthesized compounds were tested for potential anti-proliferative activity against some cell lines to evaluate the safety of PD-L1 active compounds and compare their anti-proliferative activity with that of other compounds under investigation. All compounds were found to be safe and did not have any cytotoxic effects on the fibroblast cell lines. Moreover, compounds **4**, **7**, **17,** and **30** showed little to no anti-proliferative activity against the cell lines used in this study except compound **4**, which displayed anti-proliferative activity against PC-3 (66.640%). On the other hand, compound **31** showed remarkable activities against the cell lines MCF-7, DU-145, and PC-3. Human prostate cancer cell line PC-3 is highly sensitive to some of the 32 compounds tested at 10 μM. The molecular docking study and ADMET analysis of the bioactive compounds were used to elucidate the mode-of-action mechanism.

Keywords: New sulfonamide derivatives; Salicylamide; Anisamide; PD L-1 inhibitors; Anti-proliferation assay

1. Introduction

In recent years, cancer immunotherapy has achieved great clinical success, which makes it a current topic of intensive research and brings new hope to cancer patients. Among these, the immune checkpoint inhibitor is the most mature immunotherapy and has the highest share in the market now.

Programmed cell death protein-1 or 2 and their Ligands 1 or 2 (PD-1, PD-2, PDL-1, or PDL-2) expressed on stimulated, regulatory-T lymphocytes, B, natural killers, monocytes, and dendritic cells [1,2]. PD-1 and its ligand are maintaining immune tolerance through immune inhibitory signals to T-cells [3].

PD-1 mediates tumors through interaction between the T cell-PD-1 expression and its ligand-PD-L1 on the tumor cell [4]. Monoclonal antibodies (MoAbs) against PD-1 and PD-L1 have been reported as general immune therapeutics, especially in kidney cancer. Acting as inhibitor-monotherapy or in combination with others blocked the PD-1/PD-L1 interaction [5-8].

Pembrolizumab and nivolumab are anti-PD-1 and gained approval from the Food and Drug Administration (FDA) in 2017, also; atezolizumab is an anti-PD-L1 MoAbs. The anti-PD-1 and anti-PD-L1 inhibitors have impressive antitumor effects in several malignancies. Blocking the PD-1/PD-L1 interaction stimulated cytotoxic T cells to eradicate cancer cells [9]. Toxicity with PD-1 blocking agents is less than the toxicity with previous immune therapies such as interleukin 2 and cytotoxic T-lymphocyte antigen (CTLA)-4 blockade [10]. However, immune therapeutic targeting of anti-PD-1: PD-L1/L2 also stimulated T cells against pathogens and tumors [11].

*Corresponding authors: E-mail: alaa17767@gmail.com

Receive Date: 27 September 2023, Revise Date: 11 October 2023, Accept Date: 31 October 2023

DOI: 10.21608/EJCHEM.2023.239175.8678

Compared with chemotherapy, FDA-approved PD-1/PD-L1 inhibitors have been found to cause fewer adverse events (AEs) in cancer patients who experienced no to fewer symptoms related to their treatment, less hematologic toxicity, and fewer immune-related AEs. Also, patients were less likely to discontinue treatment due to toxicities or experience treatment-related deaths. PD1/PD-L1 inhibitors are overall better tolerated than chemotherapy [12]. Expression of PD-L1 on the tumor and immune cells membrane is associated with enhanced objective response rates to PD-1/PD-L1 inhibition [13].

In addition to the MoAbs, Aurigene Discovery Technologies, and Laboratoires Pierre Fabre, in 2014, announced a collaboration license for the first peptide inhibitor of the PD-1/PD-L1 pathway. Later, it was reported that more peptides and peptidomimetics serve as inhibitors of the PD-1/PD-L1 pathway [14], and their activity relationships were also discussed [15].

Scientists from Bristol-Myers Squibb have discovered a novel series of small molecule inhibitors targeting PD-L1 [16]. These small molecule inhibitors contain a mono-ortho substituted biphenyl moiety which links to another phenyl ring via a methylene amine group. Moreover, academic research groups worldwide have made enormous efforts to develop small molecules with chemical scaffolds such as biphenyl, biaryl, urea-linked, and indole/imidazole-based as potent immune checkpoint inhibitors [15,17].

Sulfonamides are a group of drugs that have been used for a long time to treat many different diseases [18-27] and some of them work by affecting different cellular mechanisms [28-35]. Sulfonamides can also help with male erectile dysfunction [36,37]. Additionally, sulfonamides can block several important oncogenic signaling pathways [38,39].

In 2011, Sharpe et al. from Harvard University first screened small molecules containing sulfamonomethoxine and sulfamethizole scaffold that could inhibit the PD-1/PD-L1 pathway. The results showed the sulfonamide derivatives had inhibitory activity at a concentration of 10 mmol/L [40].

As the first discovered small molecule inhibitors, sulfonamides are promising as lead compounds for further modification [40,41]. The notification from Harvard et al and our experience with sulfonamides as antitumor agents have motivated us to explore a new series of sulfonamides as potential inhibitors of the PD-1/PD-L1 pathway. Further development may lead to the design of an anticancer therapy based on orally delivered immune checkpoint inhibition.

Our previous reports discussed the importance of sulfonamide new series coupled with salicylamide and/or anisamide scaffold as potent inhibitors for tubulin polymerization, dihydropteroate synthase enzyme (DHPS), and Inosine-5'-monophosphate dehydrogenase (IMPDH) [42-44]. The present study reports the virtual screening of self-database, synthesis, and biological evaluation of a series of sulfonamide derivatives coupled with salicylamide or anisamide scaffold as potential PD-L1 inhibitors. The details of compound synthesis and enzyme inhibition were discussed. Evaluation of anti-tumor of the selected compounds was also evaluated. The molecular docking study and ADMET (absorption, distribution, metabolism, excretion, and toxicity) analysis of the bioactive compounds were used to elucidate the mode-of-action mechanism.

2. Materials and Methods

2.1. Chemistry

Two series of sulfonamide derivatives (series 1 and 2) were synthesized according to the published methods [42-48].

All materials, reagents, and solvents were purchased from Sigma-Aldrich, Merck, Fisher chemicals, and Lab-Scan analytical sciences and were used without further purification. ^{1}H and ^{13}C NMR spectra were recorded at 298 K on a JEOL ECA500 spectrometer (^{1}H at 500.16 MHz and ^{13}C NMR at 125.76 MHz) and were processed using the Bruker Topspin 3.2 software. ^{1}H and ^{13}C NMR spectra were referenced to ^{1}H signals of residual non-deuterated solvents and ^{13}C signals to the deuterated solvents. ^{1}H NMR signals were reported with chemical shift values δ (ppm), multiplicity (s = singlet, d = doublet, t = triplet, q = quartet, m = multiplet and br = broad), relative integral, coupling constants J (Hz) and assignments. Mass spectra were recorded on a JEOL DART+ HI RESOLUTION mass spectrometer, and ionization of all samples was carried out using ESI. Melting points were measured on an Electrothermal IA9100 digital melting point apparatus and were uncorrected. Analytical TLC was performed on Merck silica gel 60 F254 pre-coated aluminum plates (0.2 mm) and visualized under UV light (254 nm).

Series 1 (n=1)

*2.1.1. 5-Chloro-2-methoxy-N-benzyl benzamide (**2**)*

Triethylamine (1.5 ml, 10.7 mmol) was added slowly to a solution of 5-chloro-2-methoxybenzoic acid (**1**, 2.0 g, 10.7 mmol) in dichloromethane (DCM, 20 ml) at room temperature. Ethyl chloroformate (1.02 ml, 10.7 mmol) was added dropwise to the reaction mixture, which was stirred for 1 h at room temperature. Benzylamine (1.2 ml, 10.7 mmol) was added dropwise to the reaction mixture, which was stirred at room temperature for a further 2 h. Distilled water (20 ml) was added. The organic layer was

separated, dried over anhydrous sodium sulfate, and evaporated under reduced pressure. The residue was crystallized from methanol to give transparent prism crystals (**2**; 2.85 g; yield 97%; mp 72–74°C).

2.1.2. 4-(5-chloro-2-methoxybenzamido-N-methylene) benzenesulfonyl chloride (3)

5-Chloro-2-methoxy-N-benzyl benzamide (**2**, 1.0 g, 3.6 mmol) was treated with chlorosulfonic acid (3 ml) on an ice bath with continuous stirring for 1 h. The ice bath was removed while stirring was continued overnight at room temperature. The reaction mixture was added slowly on ice to give a white precipitate. The precipitate was filtered and washed several times with distilled water until acid-free and crystallized from DCM to give white needles (**3**; 1.22 g; yield 90%; mp 113–115 °C).

2.1.3. General procedures for the synthesis of 5-chloro-2- methoxy-N-(4-sulfamoylbenzyl) benzamide derivatives (4–9)

To a solution of sodium carbonate (0.25 g, 2.36 mmol) in distilled water (3 ml) and 4-(5-chloro-2-methoxybenzamido-N-methylene) benzenesulfonyl chloride (**3**, 0.88 g, 2.35 mmol) in dichloromethane (DCM, 6 ml) was added. The appropriate amine (3.59 mmol) was added portion-wise to the reaction mixture with continuous stirring for 24 h at room temperature. The organic solvent was evaporated under a vacuum. The residue was acidified by 1N HCl. The precipitate was filtered, washed several times with distilled water and crystallized from methanol to give benzamide derivatives (**4**–**9**).

Series 2 (n=2)

The same method illustrated above was used for the synthesis of series 2 but the benzylamine was replaced with beta-phenethyl amine and finally, the benzenesulfonyl chloride derivative coupled with the appropriate amine for the synthesis of benzamides **10-19**.

2.1.3.1. 5-Chloro-2-methoxy-N-(4-(N-(4-fluorophenyl)sulfamoyl)benzyl)benzamide (4)

White granules; yield 90%; mp 212–214 °C. ^{1}H NMR (DMSO-d_6): δ 3.86 (s, 3H, OCH_3), 4.51(s, 2H, CH_2), 7.45 (d, 2H, J = 7.65 Hz, Ar–H), 7.49(d, 1H, J = 7.60 Hz, Ar–H), 7.54 (d, 1H, J = 7.65 Hz, Ar–H), 7.59(d, 2H, J = 7.65 Hz, Ar–H), 7.67-7.72 (m, 4H, Ar–H), 8.83 (s, 1H, NH), 10.23 (s, 1H, NH). ^{13}C NMR (DMSO-d_6): δ 42.91 (C-8), 56.77 (C-10), 116.20 (C-3), 123.11 (C-3″, C-5″), 123.17 (C-2″, C-6″), 123.35 (C-6), 125.54 (C-5), 125.61 (C-2′, C-6′),127.33 (C-3′, C-5′), 128.09 (C-6), 130.16 (C-1″), 132.17 (C-4), 156.37 (C-4′), 158.62 (C-1′), 160.53 (C-2), 164.54 (C-4″), 164.66(C-7). HRMS (ESI^+): m/z $[M + H]^+$ calcd. for $C_{21}H_{18}ClFN_2O_4S^+$ 448.8942 found 448.8931.

2.1.3.2. 5-Chloro-2-methoxy-N-(4-(N-(2-fluorophenyl)sulfamoyl)benzyl)benzamide (5)

Fine white crystals; yield 92%; mp 168–170 °C. ^{1}H NMR (DMSO-d_6): δ 3.86 (s, 3H, OCH3), 4.51 (d, 2H, J = 4.60 Hz, CH_2), 7.08-7.10 (m, 1H, Ar–H), 7.12 (t, 1H, J = 5.00 Hz, Ar–H), 7.14 (d, 1H, J = 5.00 Hz, Ar–H), 7.24 (d, 1H, J = 5.00 Hz, Ar–H), 7.33 (s, 1H, Ar–H), 7.46 (d, 1H, J = 5.00 Hz, Ar–H), 7.49 (d, 1H, J = 5.00 Hz, Ar–H), 7.51 (t, 1H, J = 5.00 Hz, Ar–H), 7.68-7.71 (m, 3H, Ar–H), 8.88 (s, 1H, NH), 10.19 (s, 1H, NH).^{13}C NMR (DMSO-d_6): δ 42.65 (C-8), 56.86 (C-10), 114.66 (C-3), 116.46 (C-3″), 124.93 (C-6″), 126.69 (C-1), 127.68 (C-4″), 128.02 (C-5″),128.83 (C-5), 130.14 (C-2′,C-6′), 132.17 (C-3′,C-5′), 138.98 (C-1″), 145.38 (C-4), 154.99 (C-4′), 154.99 (C-1′), 156.37 (C-2), 156.96 (C-2″), 164.66(C-7). HRMS (ESI^+): m/z $[M + H]^+$ calcd. for $C_{21}H_{18}ClFN_2O_4S^+$ 448.8942 found 448.8948.

2.1.3.3. 5-Chloro-2-methoxy-N-(4-(N-(3-fluorophenyl)sulfamoyl)benzyl)benzamide (6)

White crystals; yield 75%; mp 198–200 °C. ^{1}H NMR (400 MHz, DMSO-d_6): δ 3.86 (s, 3H, OCH_3), 4.50 (s, 2H, CH_2), 6.89 (d, 3H, J = 10.00 Hz, Ar–H), 7.16 (d, 2H, J = 10.00 Hz, Ar–H), 7.25-7.40 (m, 2H, Ar–H), 7.53 (t, 1H, J = 7.50 Hz, Ar–H), 7.54-7.65 (m, 2H, Ar–H), 7.77 (s, 1H, Ar–H), 8.83 (s, 1H, NH), 10.23 (s, 1H, NH). ^{13}C NMR (DMSO-d_6): δ 42.71 (C-8), 56.84 (C-10), 106.68 (C-2″), 106.83 (C-4″), 110.38 (C-6″), 111.00 (C-3), 114.66 (C-1), 115.80 (C-5), 125.53 (C-2′, C-6′), 129.85 (C-3′, C-5′), 130.16 (C-6), 132.20 (C-5″), 132.40 (C-4), 140.04 (C-4′), 140.14 (C-1″), 141.80 (C-1′), 156.40 (C-2), 161.79 (C-3″), 164.56 (C-7). HRMS (ESI^+): m/z $[M + H]^+$ calcd. for $C_{21}H_{18}ClFN_2O_4S^+$ 448.8942 found 448.8933.

***2.1.3.4.* 5-Chloro-2-methoxy-N-(4-(N-(2,4-difluorophenyl)sulfamoyl)benzyl)benzamide (7)**

White crystals; yield 85%; mp 212–213 °C. ^{1}H NMR (400 MHz, DMSO-d_6): δ 3.85 (s, 3H, OCH_3), 4.53 (s, 2H, CH_2), 6.96 (s, 1H, Ar–H), 7.15 (d, 2H, J = 10.00 Hz, Ar–H), 7.21 (s, 1H, Ar–H), 7.43-7.45 (m, 1H, Ar–H), 7.49 (d, 2H, J = 10.00 Hz, Ar–H), 7.64-7.66 (m, 3H, Ar–H), 8.86 (s, 1H, NH).^{13}C NMR (DMSO-d_6): δ 42.65 (C-8), 56.86 (C-10), 104.95 (C-5″), 105.15 (C-3″), 111.85 (C-3), 112.02 (C-2″), 114.66 (C-1), 127.21 (C-5), 127.94 (C-2′,C-6′), 128.30 (C-3′,C-5′), 130.13 (C-6), 132.16 (C-1″), 139.61 (C-4), 144.97 (C-4′), 156.38 (C-1′), 158.77 (C-4″), 158.86 (C-2), 160.72 (C-6″), 164.66 (C-7). HRMS (ESI^+): m/z $[M + H]^+$ calcd. for $C_{21}H_{17}ClF_2N_2O4S^+$ 466.8848 found 466.8834.

2.1.3.5. 5-Chloro-2-methoxy-N-(4-(N-(3-(trifluoromethyl)phenyl)sulfamoyl)benzyl) benzamide (8)

Yellowish white granules; yield 80%; mp 206–210 °C. ^{1}H NMR (400 MHz, DMSO-d_6): δ 3.85 (s, 3H, OCH_3), 4.49 (d, 2H, J = 5.7, CH_2), 7.17 (d, 1H, J = 10.00 Hz, Ar–H), 7.28-7.29 (m, 1H, Ar–H), 7.35 (s, 1H, Ar–H), 7.38 (d, 2H, J = 5.00 Hz, Ar–H), 7.52 (d, 2H, J = 10.00 Hz, Ar–H), 7.56 (d, 1H, J = 10.00 Hz, Ar–H), 7.63 (s, 1H, Ar–H), 7.65-7.74 (m, 2H, Ar–H), 8.85 (s, 1H, NH), 10.79 (s, 1H, NH). ^{13}C NMR (DMSO-d_6): δ 42.54 (C-8), 56.83 (C-10), 114.46 (C-2″), 116.16 (C-4″), 120.72 (C-3), 123.63 (C-1), 124.91 (C-6″), 125.23 (C-11), 125.57 (C-5), 128.84 (C-2′, C-6′), 129.88 (C-3′, C-5′), 130.17 (C-6), 130.55 (C-5″), 130.96 (C-3″), 132.21 (C-4), 132.48 (C-4′), 139.27 (C-1″), 139.96 (C-1′),156.40 (C-2), 164.53 (C-7). HRMS (ESI$^+$): m/z [M + H]$^+$ calcd. for $C_{22}H_{18}ClF_3N_2O_4S^+$ 498.9018 found 498.9022.

2.1.3.6. 5-Chloro-2-methoxy-N-(4-(N-(4-(trifluoromethyl)phenyl)sulfamoyl)benzyl) benzamide (9)

Yellowish white crystals; yield 91%; mp 192–195 °C. ^{1}H NMR (400 MHz, DMSO-d_6): δ 3.86 (s, 3H, OCH_3), 4.51 (s, 2H, CH_2), 7.15 (d, 1H, J = 5.00 Hz, Ar–H), 7.28 (m, 2H, Ar–H), 7.33 (d, 1H, J = 5.00 Hz, Ar–H), 7.47-7.50 (m, 3H, Ar–H), 7.54-7.57 (m, 2H, Ar–H), 7.67 (d, 1H, J = 5.00 Hz, Ar–H), 7.17 (d, 1H, J = 10.00 Hz, Ar–H), 7.80 (s, 1H, Ar–H), 8.85 (s, 1H, NH), 10.90 (s, 1H, NH). ^{13}C NMR (DMSO-d_6): δ 42.56 (C-8), 56.82 (C-10), 114.63 (C-3), 119.19 (C-1), 124.92 (C-2″, C-6″), 125.24 (C-10), 127.07 (C-3″, C-5″), 127.22 (C-4″), 127.35 (C-5), 128.30 (C-2′, C-6′), 128.82 (C-3′, C-5′), 130.14 (C-6), 132.18 (C-4), 138.12 (C-4′), 142.17 (C-1″), 145.85 (C-1′), 156.37 (C-2), 164.65 (C-7). HRMS (ESI$^+$): m/z [M + H]$^+$ calcd. for $C_{22}H_{18}ClF_3N_2O_4S^+$ 498.9018 found 498.9031.

2.1.3.7. 5-Chloro-2-methoxy-N-(4-(N-(4-chlorophenyl)sulfamoyl)phenethyl)benzamide (10)

White crystals; yield 92%; mp 188–190 °C. ^{1}H NMR (400 MHz, DMSO-d_6): δ 2.85 (t, 2H, J = 6.67 Hz, CH_2), 3.48 (t, 2H, J = 6.65 Hz, CH_2), 3.73 (s, 3H, OCH_3), 7.06 (d, 2H, J = 10.00 Hz, Ar–H), 7.07-7.09 (m, 1H, Ar–H), 7.22 (d, 2H, J = 10.00 Hz, Ar–H), 7.28-7.32 (m, 2H, Ar–H), 7.40 (d, 1H, J = 5.00 Hz, Ar–H), 7.45 (d, 1H, J = 5.00 Hz, Ar–H), 7.58 (d, 1H, J = 5.00 Hz, Ar–H), 7.67 (d, 1H, J = 5.00 Hz, Ar–H), 8.20 (s, 1H, NH). ^{13}C NMR (DMSO-d_6): δ 35.14 (C-9), 42.04 (C-8), 56.68 (C-10), 114.66 (C-3), 122.04 (C-1), 124.91 (C-2″, C-6″), 125.26 (C-5), 127.25 (C-4″), 128.28 (C-2′, C-6′), 128.83 (C-3′, C-5′), 129.55 (C-6), 130.05 (C-3″, C-5″),), 130.09 (C-4), 132.06 (C-1″), 137.80 (C-4′), 145.45 (C-1′), 156.20 (C-2), 164.17 (C-7). HRMS (ESI$^+$): m/z [M + H]$^+$ calcd. for $C_{22}H_{20}Cl2N_2O_4S$+ 479.3754 found 479.3744.

2.1.3.8. 5-Chloro-2-methoxy-N-(4-(N-phenylsulfamoyl)phenethyl)benzamide (11)

Yellowish white crystals; yield 95%; mp 185–186 °C. ^{1}H NMR (400 MHz, DMSO-d_6): δ 2.85 (t, 2H, J = 6.65 Hz, CH_2), 3.48 (t, 2H, J = 6.65 Hz, CH_2),3.66 (s, 3H, OCH_3), 6.97 (t, 1H, J = 5.00 Hz, Ar–H), 7.06-7.11 (m, 2H, Ar–H), 7.18 (t, 2H, J = 7.50 Hz, Ar–H), 7.32 (s, 1H, Ar–H), 7.38-7.40 (m, 2H, Ar–H), 7.45 (d, 1H, J = 5.00 Hz, Ar–H), 7.48 (d, 1H, J = 10.00 Hz, Ar–H), 7.60 (d, 1H, J = 5.00 Hz, Ar–H), 7.69 (d, 1H, J = 5.00 Hz, Ar–H), 8.20 (s, 1H, NH), 10.26 (s, 1H, NH). ^{13}C NMR (DMSO-d_6): δ 35.11 (C-9), 42.15 (C-8), 56.44 (C-10), 114.66 (C-3), 120.44 (C-2″, C-6″), 124.46 (C-1), 124.92 (C-4″), 125.32 (C-5), 127.28 (C-2′, C-6′), 129.63 (C-3′, C-5′), 130.05 (C-6), 130.25 (C-1″), 132.02 (C-3″, C-5″), 138.14 (C-4), 138.32 (C-4′), 145.41 (C-1′), 156.20 (C-2), 164.11 (C-7). HRMS (ESI$^+$): m/z [M + H]$^+$ calcd. for $C_{22}H_{21}ClN_2O_4S^+$ 444.9303 found 444.9312.

2.1.3.9. 5-Chloro-2-methoxy-N-(4-(N-(4-fluorophenyl)sulfamoyl)phenethyl)benzamide (12)

white crystals; yield 94%; mp 174–176 °C. ^{1}H NMR (400 MHz, DMSO-d_6): δ 2.85 (t, 2H, J = 7.70 Hz, CH_2), 3.49(t, 2H, J = 7.70 Hz, CH_2),3.71 (s, 3H, OCH_3), 7.03 (d, 1H, J = 5.00 Hz, Ar–H), 7.08 (d, 3H, J = 5.00 Hz, Ar–H), 7.40 (s, 1H, Ar–H), 7.44 (d, 2H, J = 5.00 Hz, Ar–H), 7.60 (d, 1H, J = 5.00 Hz, Ar–H), 7.63-7.66 (m, 3H, Ar–H), 8.21 (s, 1H, NH), 10.21 (s, 1H, NH).^{13}C NMR (DMSO-d_6): δ 35.13 (C-9), 42.10 (C-8), 56.43 (C-10), 114.63 (C-3), 116.24 (C-3″,C-5″), 116.42 (C-2″,C-6″), 123.19 (C-1), 123.26 (C-5), 124.95 (C-2′,C-6′), 127.29 (C-3′,C-5′), 130.09 (C-6), 132.02(C-1″), 134.49 (C-4), 145.48 (C-4′), 156.20 (C-1′), 158.61 (C-2), 160.53 (C-2), 164.12 (C-7). HRMS (ESI$^+$): m/z [M + H]$^+$ calcd. for $C_{22}H_{20}ClFN_2O_4S^+$ 462.9208 found 462.9221.

2.1.3.10. 5-Chloro-2-methoxy-N-(4-(N-(2-fluorophenyl)sulfamoyl)phenethyl)benzamide (13)

Fine white crystals; yield 91%; mp 157–160 °C. ^{1}H NMR (400 MHz, DMSO-d_6): δ 2.88 (t, 2H, J = 7.50 Hz, CH_2), 3.70 (t, 2H, J = 7.50 Hz, CH_2),3.76 (s, 3H, OCH_3), 7.08 (d, 1H, J = 10.00 Hz, Ar–H), 7.10-7.13 (m, 3H, Ar–H), 7.38 (d, 1H, J = 10.00 Hz, Ar–H), 7.45 (d, 1H, J = 5.00 Hz, Ar–H), 7.53 (t, 1H, J = 7.50 Hz, Ar–H), 7.56 (s, 1H, Ar–H), 7.62 (d, 2H, J = 10.00 Hz, Ar–H), 7.66 (t, 1H, J = 10.00 Hz, Ar–H), 8.20 (s, 1H, NH), 10.04 (s, 1H, NH). ^{13}C NMR (DMSO-d_6): δ 35.24 (C-9), 42.32 (C-8), 56.75 (C-10), 114.69 (C-3), 116.45 (C-5″), 116.58 (C-2″), 124.91 (C-1), 124.96 (C-4″), 125.12 (C-3″), 125.38 (C-5), 126.72 (C-2′, C-6′), 127.21 (C-3′,C-5′), 127.64 (C-6), 130.00 (C-1″),

132.03 (C-4), 138.52 (C-4′), 145.49 (C-1′), 155.06 (C-2), 156.23 (C-6″), 164.15 (C-7). HRMS (ESI^+): m/z $[M + H]^+$ calcd. for $C_{22}H_{20}ClFN_2O_4S^+$ 462.9208 found 462.9017.

2.1.3.11. 5-Chloro-2-methoxy-N-(4-(N-(3-fluorophenyl)sulfamoyl)phenethyl)benzamide (14)

White crystals; yield 67%; mp 169–170 °C. ^1H NMR (400 MHz, DMSO-d_6): δ 2.86 (t, 2H, J = 6.70 Hz, CH_2), 3.49 (t, 2H, J = 5.75 Hz, CH_2),3.73 (s, 3H, OCH_3), 6.79 (t, 1H, J = 7.50 Hz, Ar–H), 6.90 (d, 2H, J = 5.00 Hz, Ar–H), 7.06 (s, 1H, Ar–H), 7.07 (s, 1H, Ar–H), 7.19 (d, 1H, J = 5.00 Hz, Ar–H), 7.31 (d, 1H, J = 5.00 Hz, Ar–H), 7.42 (d, 1H, J = 5.00 Hz, Ar–H), 7.60 (d, 1H, J = 5.00 Hz, Ar–H), 7.74 (d, 2H, J = 5.00 Hz, Ar–H), 8.20 (s, 1H, NH). ^{13}C NMR (DMSO-d_6): δ 35.11 (C-9), 42.06 (C-8), 56.63 (C-10), 110.95 (C-2″), 114.63 (C-4″), 124.95 (C-6″), 126.54 (C-3), 127.31 (C-1), 128.83 (C-5), 130.30 (C-2′, C-6′), 131.37 (C-3′, C-5′), 132.46 (C-6), 133.06 (C-5″), 137.69 (C-4), 140.26 (C-4′), 145.75 (C-1″), 156.15 (C-1′), 161.81 (C-2), 163.74 (C-4″), 164.17 (C-7). HRMS (ESI^+): m/z $[M + H]^+$ calcd. for $C_{22}H_{20}ClFN_2O_4S^+$ 462.9208 found 462.9020.

2.1.3.12. 5-Chloro-2-methoxy-N-(4-(N-(4-(trifluoromethyl)phenyl)sulfamoyl)phenethyl) benzamide (15)

Orange crystals; yield 60%; mp 186–188 °C. ^1H NMR (400 MHz, DMSO-d_6): δ 2.85 (t, 2H, J = 7.60 Hz, CH_2), 3.47 (t, 2H, J = 6.70 Hz, CH_2),3.67 (s, 3H, OCH_3), 7.09 (d, 1H, J = 10.00 Hz, Ar–H), 7.20 (d, 2H, J = 5.00 Hz, Ar–H), 7.33 (s, 1H, Ar–H), 7.41 (d, 1H, J = 10.00 Hz, Ar–H), 7.45 (d, 1H, J = 5.00 Hz, Ar–H), 7.47 (d, 1H, J = 5.00 Hz, Ar–H), 7.51 (d, 1H, J = 10.00 Hz, Ar–H), 7.57 (d, 1H, J = 5.00 Hz, Ar–H), 7.74 (d, 2H, J = 10.00 Hz, Ar–H), 8.20 (s, 1H, NH). ^{13}C NMR (DMSO-d_6): δ 35.22 (C-9), 42.12 (C-8), 56.45 (C-10), 114.62 (C-3), 119.19 (C-1), 123.11 (C-2″, C-6″), 124.91 (C-4″), 125.29 (C-3″, C-5″), 127.27 (C-7'), 128.84 (C-5), 130.02 (C-2′, C-6′), 130.30 (C-3′, C-5′), 133.11 (C-6), 132.04 (C-4), 137.74 (C-4′), 142.16 (C-1″), 145.93 (C-1′), 156.19 (C-2), 164.19 (C-7). HRMS (ESI^+): m/z $[M + H]^+$ calcd. for $C_{23}H_{20}ClF_3N_2O_4S^+$ 512.9283 found 512.9277.

2.1.3.13. 5-Chloro-2-methoxy-N-(4-(N-(4-bromophenyl)sulfamoyl)phenethyl)benzamide (16)

White crystals; yield 80%; mp 187–188 °C. ^1H NMR (400 MHz, DMSO-d_6): δ 2.86 (t, 2H, J = 7.50 Hz, CH_2), 3.47 (t, 2H, J = 7.50 Hz, CH_2),3.80 (s, 3H, OCH_3), 7.03 (d, 2H, J = 5.00 Hz, Ar–H), 7.08 (d, 1H, J = 10.00 Hz, Ar–H), 7.31 (s, 1H, Ar–H), 7.36 (d, 2H, J = 5.00 Hz, Ar–H), 7.41 (d, 2H, J = 10.00 Hz, Ar–H), 7.45 (d, 1H, J = 5.00 Hz, Ar–H), 7.60 (d, 1H, J = 5.00 Hz, Ar–H), 7.70 (d, 1H, J = 10.00 Hz, Ar–H), 8.12 (s, 1H, NH), 10.30 (s, 1H, NH). ^{13}C NMR (DMSO-d_6): δ 35.20 (C-9), 42.14 (C-8), 56.25 (C-10), 100.50 (C-3), 114.62 (C-4″), 116.64 (C-1), 122.28 (C-2″, C-6″), 127.27 (C-5), 128.83 (C-2′, C-6′), 130.09 (C-3′, C-5′), 130.16 (C-6), 132.07 (C-3″, C-5″), 132.53 (C-4), 134.08 (C-1″), 137.74 (C-4′), 145.66 (C-1′), 156.19 (C-2), 164.16 (C-7). HRMS (ESI^+): m/z $[M + H]^+$ calcd. for $C_{22}H_{20}BrClN_2O_4S^+$ 523.8263 found 523.8277.

2.1.3.14. 5-Chloro-2-methoxy-N-(4-(N-(4-methylphenyl)sulfamoyl)phenethyl)benzamide (17)

White crystals; yield 84%; mp 199–200 °C. ^1H NMR (400 MHz, DMSO-d_6): δ 2.83 (t, 2H, J = 7.50 Hz, CH_2), 3.47 (t, 2H, J = 7.50 Hz, CH_2),3.69 (s, 3H, OCH_3), 6.95-7.10 (m, 4H, Ar–H), 7.38 (d, 2H, J = 5.00 Hz, Ar–H), 7.46 (d, 2H, J = 5.00 Hz, Ar–H), 7.59 (s, 1H, Ar–H), 7.65 (d, 2H, J = 10.00 Hz, Ar–H), 8.00 (s, 1H, NH), 10.07 (s, 1H, NH). ^{13}C NMR (DMSO-d_6): δ 20.79 (C-7″), 35.26 (C-9), 42.43 (C-8), 56.71 (C-10), 114.68 (C-3), 121.05 (C-2″, C-6″), 124.92 (C-1), 125.35 (C-5), 127.27 (C-2′, C-6′), 128.84 (C-3′, C-5′), 129.97 (C-6), 130.04 (C-3″, C-5″), 132.02 (C-4″), 133.79 (C-4), 135.62 (C-1″), 138.16 (C-4′), 145.27 (C-1′), 156.22 (C-2), 164.10 (C-7). HRMS (ESI^+): m/z $[M + H]^+$ calcd. for $C_{23}H_{23}ClN_2O_4S^+$ 458.9568 found 458.9559.

2.1.3.15. 5-Chloro-2-methoxy-N-(4-(N-benzylsulfamoyl)phenethyl)benzamide (18)

White crystals; yield 82%; mp 118–120 °C. ^1H NMR (400 MHz, DMSO-d_6): δ 2.90 (t, 2H, J = 13.31 Hz, CH_2), 3.52 (t, 2H, J = 13.32 Hz, CH_2), 3.80 (s, 2H, CH_2), 3.95 (s, 3H, OCH_3), 7.12-7.14 (m, 2H, Ar–H), 7.22 (t, 3H, J = 5.00 Hz, Ar–H), 7.27 (d, 2H, J = 5.00 Hz, Ar–H), 7.45 (s, 1H, Ar–H), 7.46 (d, 1H, J = 5.00 Hz, Ar–H), 7.49 (d, 1H, J = 5.00 Hz, Ar–H), 7.68 (d, 1H, J = 5.00 Hz, Ar–H), 7.75 (d, 1H, J = 5.00 Hz, Ar–H), 8.20 (s, 1H, NH), 8.60 (s, 1H, NH). ^{13}C NMR (DMSO-d_6): δ 35.28 (C-9), 42.31 (C-8), 46.71 (C-7′), 56.81 (C-10), 114.70 (C-3), 122.03 (C-1), 124.83 (C-4″), 127.27 (C-5), 127.14 (C-2″, C-6″), 127.66 (C-2′, C-6′), 128.10 (C-3′, C-5′), 128.74 (C-5″), 129.99 (C-6), 130.14 (C-4), 132.11 (C-4′), 138.19 (C-1″), 144.83 (C-1′),156.29 (C-2), 164.16 (C-7). HRMS (ESI^+): m/z $[M + H]^+$ calcd. for $C_{23}H_{23}ClN_2O_4S^+$ 458.9568 found 458.9571.

2.1.3.16. 5-Chloro-2-methoxy-N-(4-(N-phenethylsulfamoyl)phenethyl)benzamide (19)

Yellowish white crystals; yield 63%; mp 121–124 °C. ^1H NMR (400 MHz, DMSO-d_6): δ 2.65 (t, 2H, J = 13.00 Hz, CH_2), 2.91 (t, 2H, J = 13.00 Hz, CH_2), 3.52 (t, 2H, J = 13.30 Hz, CH_2), 3.75 (t, 2H, J = 13.30 Hz, CH_2), 3.80 (s, 3H, OCH_3), 7.11 (d, 2H, J = 5.00 Hz, Ar–H), 7.14-7.21 (m, 3H, Ar–H), 7.41-7.45 (m, 3H, Ar–H), 7.63 (s, 1H, Ar–H), 7.65-7.71

(m, 3H, Ar–H), 8.42 (s, 1H, NH).^{13}C NMR (DMSO-d_6): δ 35.44 (C-8′), 36.11 (C-9), 42.66 (C-7′), 46.19 (C-8), 56.76 (C-10), 114.66 (C-3), 122.33 (C-1), 124.76 (C-4″), 125.21 (C-5), 127.15 (C-2″,C-6″), 128.82 (C-2′,C-6′), 129.13 (C-3′,C-5′), 130.01 (C-6), 130.12 (C-3″,C-5″), 132.11 (C-4), 138.90 (C-4′), 139.23 (C-1″), 144.82 (C-1′), 156.29 (C-2), 164.14 (C-7). HRMS (ESI^+): m/z $[M + H]^+$ calcd. for $C_{24}H_{25}ClN_2O_4S^+$ 458.9568 found 458.9565.

2.1.4. General synthetic procedures of 5-chloro-N-(4-sulfamoylbenzyl) salicylamide derivatives ***(20–35)*** *Potass*ium cyanide (0.29 g, 6 mmol) and the appropriate benzamide derivatives [(**4**–**19**), 4 mmol] were added to anhydrous dimethyl sulfoxide (5 ml). The reaction mixture was refluxed for 1 h under stirring and then cold water (50 ml) was added to the reaction mixture. The solution was acidified with 1N HCl, the precipitate was filtered, washed several times with distilled water and crystallized from benzene to give salicylamide derivatives (**20**–**35**).

2.1.4.1. 5-Chloro-N-(4-(N-(4-fluorophenyl) sulfamoyl)benzyl)salicylamide (20)

Fine brown crystals; yield 98%; mp 174-177 °C. ^{1}H NMR (DMSO-d_6): δ 4.76(s, 2H, CH_2), 6.96 (d, 2H, J = 5.00 Hz, Ar–H), 7.07 (d, 3H, J = 5.00 Hz, Ar–H), 7.49 (d, 2H, J = 10.00 Hz, Ar–H), 7.55-7.60 (m, 2H, Ar–H), 7.70 (s, 1H, Ar–H), 7.91-7.93 (m, 2H, Ar–H), 9.40 (s, 1H, NH), 10.25 (s, 1H, NH), 12.38 (s, 1H, OH). ^{13}C NMR (DMSO-d_6): δ 42.90 (C-8), 116.19 (C-3), 117.46 (C-3″, C-5″), 119.84 (C-2″, C-6″), 123.49 (C-6), 127.42 (C-5), 128.37 (C-2′, C-6′),129.84 (C-3′, C-5′), 133.91 (C-6), 134.45 (C-1″), 138.51 (C-4), 140.89 (C-4′), 158.90 (C-1′), 159.02 (C-2), 160.53 (C-4″), 168.08(C-7). HRMS (ESI^+): m/z $[M + H]^+$ calcd. for $C_{20}H_{16}ClFN2O_4S^+$ 434.8678 found 448.8692.

2.1.4.2. 5-Chloro-N-(4-(N-(2-fluorophenyl) sulfamoyl)benzyl)salicylamide (21)

white crystals; yield 99%; mp 217-218 °C. ^{1}H NMR (DMSO-d_6): δ 4.55(d, 1H, J = 5.70 Hz, CH_2), 6.94 (d, 1H, J = 10.00 Hz, Ar–H), 7.07 (t, 2H, J = 5.00 Hz, Ar–H), 7.13 (d, 2H, J = 10.00 Hz, Ar–H), 7.22 (d, 1H, J = 5.00 Hz, Ar–H), 7.43 (d, 2H, J = 10.00 Hz, Ar–H), 7.47 (d, 1H, J = 10.00 Hz, Ar–H), 7.67 (s, 1H, Ar–H), 7.93 (d, 1H, J = 5.00 Hz, Ar–H), 9.39 (s, 1H, NH), 10.16 (s, 1H, NH), 12.31 (s, 1H, OH).^{13}C NMR (DMSO-d_6): δ 42.63 (C-8), 116.63 (C-3), 117.46 (C-3″), 119.84 (C-6″), 122.99 (C-1), 125.01 (C-4″), 125.18 (C-5″),126.70 (C-5), 127.31 (C-2′,C-6′), 127.71 (C-3′,C-5′), 128.10 (C-1″), 128.30 (C-4), 133.89 (C-4′), 138.50 (C-1′), 144.58 (C-2), 156.88 (C-2″), 168.04(C-7). HRMS (ESI^+): m/z $[M + H]^+$ calcd. for $C_{20}H_{16}ClFN_2O_4S^+$ 434.8678 found 448.8671.

2.1.4.3. 5-Chloro-N-(4-(N-(3-fluorophenyl) sulfamoyl)benzyl)salicylamide (22)

Fine brown crystals; yield 98%; mp 178-182 °C. ^{1}H NMR (400 MHz, DMSO-d_6): δ 4.54 (s, 1H, CH_2), 6.81 (d, 1H, J = 5.00 Hz, Ar–H), 6.90-6.92 (m, 2H, Ar–H), 7.17 (t, 1H, J = 7.50 Hz, Ar–H), 7.42 (d, 1H, J = 5.00 Hz, Ar–H), 7.50 (d, 2H, J = 10.00 Hz, Ar–H), 7.68 (s, 1H, Ar–H), 7.77 (s, 1H, Ar–H), 7.93-7.94 (m, 2H, Ar–H), 9.40 (s, 1H, NH), 10.62 (s, 1H, NH), 12.33 (s, 1H, OH). ^{13}C NMR (DMSO-d_6): δ 42.11 (C-8), 106.59 (C-2″), 106.79 (C-4″), 110.85 (C-6″), 111.01 (C-3), 115.72 (C-1), 119.83 (C-5), 123.01 (C-2′, C-6′), 127.44 (C-3′, C-5′), 128.22 (C-6), 128.51 (C-5″), 131.50 (C-4), 133.88 (C-4′), 138.11 (C-1″), 144.86 (C-1′), 158.92 (C-2), 163.77 (C-3″), 168.10 (C-7). HRMS (ESI^+): m/z $[M + H]^+$ calcd. for $C_{20}H_{16}ClFN_2O_4S^+$ 434.8678 found 448.8688.

2.1.4.4. 5-Chloro-N-(4-(N-(2,4-difluorophenyl) sulfamoyl)benzyl)salicylamide (23)

Fine yellowish white crystals; yield 99%; mp 191-194 °C. ^{1}H NMR (400 MHz, DMSO-d_6): δ 4.55 (s, 1H, CH_2), 7.00-7.94 (m, 10H, Ar–H), 9.93 (s, 1H, NH), 10.28 (s, 1H, NH), 12.40 (s, 1H, OH).^{13}C NMR (DMSO-d_6): δ 42.55 (C-8), 105.16 (C-5″), 112.15 (C-3″), 117.53 (C-3), 119.87 (C-2″), 121.44 (C-1), 123.00 (C-5), 125.76 (C-2′,C-6′), 127.35 (C-3′,C-5′), 128.32 (C-6), 129.14 (C-1″), 133.91 (C-4), 139.08 (C-4′), 144.66 (C-1′), 155.85 (C-4″), 158.92 (C-2), 159.56 (C-6″), 168.06 (C-7). HRMS (ESI^+): m/z $[M + H]^+$ calcd. for $C_{20}H_{15}ClF_2N_2O_4S^+$ 452.8583 found 452.8595.

2.1.4.5. 5-Chloro-N-(4-(N-(3-(trifluoromethyl) phenyl)sulfamoyl)benzyl)salicylamide (24)

Fine brown crystals; yield 97%; mp 176-178 °C. ^{1}H NMR (400 MHz, DMSO-d_6): δ 4.52 (s, 1H, CH_2), 6.93-7.91 (m, 11H, Ar–H), 9.39 (s, 1H, NH), 10.77 (s, 1H, NH), 12.30 (s, 1H, OH).^{13}C NMR (DMSO-d_6): δ 42.34 (C-8), 114.46 (C-2″), 116.16 (C-4″), 117.46 (C-3), 119.83 (C-1), 120.83 (C-6″), 122.97 (C-14), 123.55 (C-5), 127.40 (C-2′,C-6′), 128.09 (C-3′,C-5′), 128.55 (C-6), 130.55 (C-5″), 131.10 (C-3″), 132.21 (C-4), 133.88.48 (C-4′), 139.23 (C-1″), 145.03 (C-1′),158.89 (C-2), 168.05 (C-7). HRMS (ESI^+): m/z $[M + H]^+$ calcd. for $C_{21}H_{16}ClF_3N_2O_4S^+$ 484.8752 found 484.8748.

2.1.4.6. 5-Chloro-N-(4-(N-(4-(trifluoromethyl) phenyl)sulfamoyl)benzyl)salicylamide (25)

Yellowish white crystals; yield 99%; mp 108-110 °C. ^{1}H NMR (400 MHz, DMSO-d_6): δ 4.52 (s, 1H, CH_2), 6.91 (d, 1H, J = 5.00 Hz, Ar–H), 7.26 (d, 2H, J = 5.00 Hz, Ar–H), 7.33-7.35 (m, 2H, Ar–H), 7.48 (d, 2H, J = 10.00 Hz, Ar–H), 7.57 (d, 2H, J = 5.00 Hz, Ar–H), 7.78 (d, 1H, J = 5.00 Hz, Ar–H), 7.90 (s, 1H, Ar–H),

9.39 (s, 1H, NH), 10.91 (s, 1H, NH), 12.30 (s, 1H, OH). ^{13}C NMR (DMSO-d_6): δ 42.45 (C-8), 117.48 (C-3), 119.18 (C-1), 119.83 (C-2″, C-6″), 122.99 (C-14), 124,88.07 (C-3″, C-5″), 125.11 (C-4″), 127.10 (C-5), 127.41 (C-2′, C-6′), 128.10 (C-3′, C-5′), 128.59 (C-6), 133.89 (C-4), 138.38 (C-4′), 142.13 (C-1″), 145.05 (C-1′), 158.85 (C-2), 168.02 (C-7). HRMS (ESI$^+$): m/z [M + H]$^+$ calcd. for $C_{21}H_{16}ClF_3N_2O_4S^+$ 484.8752 found 484.8761.

2.1.4.7. 5-Chloro-N-(4-(N-(4-chlorophenyl) sulfamoyl)phenethyl)salicylamide (26)

Fine white crystals; yield 96%; mp 78–80 °C. ^{1}H NMR (400 MHz, DMSO-d_6): δ 2.88 (t, 2H, J = 6.67 Hz, CH_2), 3.49 (t, 2H, J = 5.75 Hz, CH_2), 6.91 (d, 1H, J = 10.00 Hz, Ar–H), 7.06 (d, 2H, J = 10.00 Hz, Ar–H), 7.24 (d, 2H, J = 10.00 Hz, Ar–H), 7.40 (d, 3H, J = 5.00 Hz, Ar–H), 7.66 (d, 2H, J = 10.00 Hz, Ar–H), 6.91 (s, 1H, Ar–H), 8.89 (s, 1H, NH), 10.37 (s, 1H, NH), 12.45, OH). ^{13}C NMR (DMSO-d_6): δ 35.12 (C-9), 42.14 (C-8), 118.11 (C-3), 119.82 (C-1), 122.19 (C-2″, C-6″), 122.86 (C-5), 127.29 (C-4″), 127.77 (C-2′, C-6′), 128.70 (C-3′, C-5′), 129.61 (C-6), 130.09 (C-3″, C-5″),), 133.74 (C-4), 137.24 (C-1″), 137.80 (C-4′), 145.39 (C-1′), 158.97 (C-2), 167.94 (C-7). HRMS (ESI$^+$): m/z [M + H]$^+$ calcd. for $C_{21}H_{18}Cl_2N_2O_4S^+$ 465.3488 found 465.3482.

2.1.4.8. 5-Chloro-N-(4-(N-phenylsulfamoyl) phenethyl)salicylamide (27)

Fine brown crystals; yield 95%; mp 179–180 °C. ^{1}H NMR (400 MHz, DMSO-d_6): δ 2.87 (t, 2H, J = 6.65 Hz, CH_2), 3.49 (t, 2H, J = 6.65 Hz, CH_2), 6.97 (t, 1H, J = 7.50 Hz, Ar–H), 7.02 (t, 1H, J = 5.00 Hz, Ar–H), 7.12 (d, 1H, J = 5.00 Hz, Ar–H), 7.18 (t, 1H, J = 10.00 Hz, Ar–H), 7.35 (d, 1H, J = 5.00 Hz, Ar–H), 7.39 (s, 1H, Ar–H), 7.42 (d, 1H, J = 10.00 Hz, Ar–H), 7.64 (d, 1H, J = 10.00 Hz, Ar–H), 7.67 (d, 1H, J = 10.00 Hz, Ar–H), 7.70 (d, 1H, J = 5.00 Hz, Ar–H), 7.80-7.81 (m, 1H, Ar–H), 7.85 (d, 1H, J = 5.00 Hz, Ar–H), 8.93 (s, 1H, NH), 10.27 (s, 1H, NH), 12.52 (s, 1H, OH). ^{13}C NMR (DMSO-d_6): δ 35.14 (C-9), 42.11 (C-8), 117.40 (C-3), 119.88 (C-2″, C-6″), 120.64 (C-1), 122.93 (C-4″), 124.58 (C-5), 127.41 (C-2′, C-6′), 127.78 (C-3′, C-5′), 129.66 (C-6), 130.03 (C-1″), 133.79 (C-3″, C-5″), 138.27 (C-4), 145.20 (C-4′), 159.07 (C-1′), 168.05 (C-2), 168.29 (C-7). HRMS (ESI$^+$): m/z [M + H]$^+$ calcd. for $C_{21}H_{19}ClN_2O_4S^+$ 430.9038 found 430.9051.

2.1.4.9. 5-Chloro-N-(4-(N-(4-fluorophenyl) sulfamoyl)phenethyl)salicylamide (28)

Fine brown crystals; yield 99%; mp 68–70 °C. ^{1}H NMR (400 MHz, DMSO-d_6): δ 2.87 (t, 2H, J = 7.60 Hz, CH_2), 3.49(t, 2H, J = 7.60 Hz, CH_2), 6.90-7.83 (m, 11H, Ar–H), 8.89 (s, 1H, NH), 10.16 (s, 1H, NH), 12.46 (s, 1H, OH).^{13}C NMR (DMSO-d_6): δ 35.34 (C-9), 42.40 (C-8), 116.26 (C-3), 119.83 (C-3″,C-5″), 123.41 (C-2″,C-6″), 127.32 (C-1), 127.78 (C-5), 128.10 (C-2′,C-6′), 130.05 (C-3′,C-5′), 133.76 (C-6), 134.46 (C-1″), 145.24 (C-4), 156.22 (C-4′), 159.02 (C-1′), 160.57 (C-2), 163.82 (C-2), 167.96 (C-7). HRMS (ESI$^+$): m/z [M + H]$^+$ calcd. for $C_{21}H_{18}ClFN_2O_4S^+$ 448.8942 found 448.8935.

2.1.4.10. 5-Chloro-N-(4-(N-(2-fluorophenyl) sulfamoyl)phenethyl)salicylamide (29)

Yellowish white crystals; yield 90%; mp 69–71 °C. ^{1}H NMR (400 MHz, DMSO-d_6): δ 2.90 (t, 2H, J = 6.70 Hz, CH_2), 3.52 (t, 2H, J = 7.60 Hz, CH_2), 6.93-6.94 (m, 1H, Ar–H), 7.11 (t, 2H, J = 12.5 Hz, Ar–H), 7.15-7.17 (m, 2H, Ar–H), 7.38-7.40 (m, 2H, Ar–H), 7.60-7.62 (m, 2H, Ar–H), 7.83-7.85 (m, 2H, Ar–H), 8.90 (s, 1H, NH), 10.10 (s, 1H, NH), 12.48 (s, 1H, OH). ^{13}C NMR (DMSO-d_6): δ 35.14 (C-9), 42.22 (C-8), 116.41 (C-3), 116.57 (C-5″), 122.86 (C-2″), 123.18 (C-1), 125.11 (C-4″), 126.92 (C-3″), 127.25 (C-5), 127.78 (C-2′, C-6′), 129.95 (C-3′, C-5′), 133.76 (C-6), 135.52 (C-1″), 138.12 (C-4), 145.22 (C-4′), 155.16 (C-1′), 157.13 (C-2), 159.02 (C-6″), 167.95 (C-7). HRMS (ESI$^+$): m/z [M + H]$^+$ calcd. for $C_{21}H_{18}ClFN_2O_4S^+$ 448.8942 found 448.8930.

2.1.4.11. 5-Chloro-N-(4-(N-(3-fluorophenyl) sulfamoyl)phenethyl)salicylamide (30)

Fine brown crystals; yield 90%; mp 183–184 °C. ^{1}H NMR (400 MHz, DMSO-d_6): δ 2.89 (t, 2H, J =7.65 Hz, CH_2), 3.50 (t, 2H, J =7.65 Hz, CH_2), 6.79-7.84 (m, 11H, Ar–H), 8.89 (s, 1H, NH), 10.54 (s, 1H, NH), 12.45 (s, 1H, OH). ^{13}C NMR (DMSO-d_6): δ 35.12 (C-9), 42.17 (C-8), 106.88 (C-2″), 110.82 (C-4″), 115.79 (C-6″), 117.34 (C-3), 119.81 (C-1), 122.86 (C-5), 127.76 (C-2′, C-6′), 130.15 (C-3′, C-5′), 131.42 (C-6), 133.72 (C-5″), 137.81 (C-4), 140.23 (C-4′), 145.50 (C-1″), 159.03 (C-1′), 161.81 (C-2), 163.75 (C-4″), 167.99 (C-7). HRMS (ESI$^+$): m/z [M + H]$^+$ calcd. for $C_{21}H_{18}ClFN_2O_4S^+$ 448.8942 found 448.8949.

2.1.4.12. 5-Chloro-N-(4-(N-(4-(trifluoromethyl) phenyl)sulfamoyl)phenethyl)salicylamide (31)

White crystals; yield 92%; mp 98–100 °C. ^{1}H NMR (400 MHz, DMSO-d_6): δ 2.88 (t, 2H, J = 7.60 Hz, CH_2), 3.50 (t, 2H, J = 6.70 Hz, CH_2), 6.89-7.83 (m, 11H, Ar–H), 8.89 (s, 1H, NH), 10.90 (s, 1H, NH), 12.39 (s, 1H, OH). ^{13}C NMR (DMSO-d_6): δ 35.02 (C-9), 42.10 (C-8), 117.34 (C-3), 119.28 (C-1), 119.81 (C-2″, C-6″), 122.83 (C-4″), 127.04 (C-3″, C-5″), 127.30 (C-14), 130.25 (C-5), 133.25 (C-2′, C-6′), 134.13 (C-3′, C-5′), 135.04 (C-6), 137.83 (C-4), 140.16 (C-4′), 142.34 (C-1″), 145.67 (C-1′), 159.01 (C-2), 167.97 (C-7). HRMS (ESI$^+$): m/z [M + H]$^+$ calcd. for $C_{22}H_{18}ClF_3N_2O_4S^+$ 498.9018 found 498.9033.

2.1.4.13. 5-Chloro-N-(4-(N-(4-bromophenyl) sulfamoyl)phenethyl)salicylamide (32)

Yellowish white crystals; yield 99%; mp 92–94 °C. ^{1}H NMR (400 MHz, DMSO-d_6): δ 2.91 (t, 2H, J = 6.65 Hz, CH_2), 3.53 (t, 2H, J = 7.60 Hz, CH_2), 7.00-7.86 (m, 11H, Ar–H), 8.90 (s, 1H, NH). ^{13}C NMR (DMSO-d_6): δ 35.70 (C-9), 42.44 (C-8), 100.00 (C-3), 117.13 (C-4″), 119.84 (C-1), 122.42 (C-2″, C-6″), 122.84 (C-5), 127.30 (C-2′, C-6′), 127.78 (C-3′, C-5′), 128.04 (C-6), 130.13 (C-3″, C-5″), 132.54 (C-4), 133.76 (C-1″), 137.73 (C-4′), 145.42 (C-1′), 159.01 (C-2), 167.95 (C-7). HRMS (ESI$^+$): m/z [M + H]$^+$ calcd. for $C_{21}H_{18}BrClN_2O_4S^+$ 509.7998 found 509.7991.

2.1.4.14. 5-Chloro-N-(4-(N-(4-methylphenyl) sulfamoyl)phenethyl)salicylamide (33)

Fine yellowish white crystals; yield 91%; mp 87–90 °C. ^{1}H NMR (400 MHz, DMSO-d_6): δ 2.21 (s, 3H, CH_3), 2.86 (t, 2H, J = 6.60 Hz, CH_2), 3.49 (t, 2H, J = 7.00 Hz, CH_2), 6.94 (d, 5H, J =10 Hz, Ar–H), 7.32-7.35 (m, 3H, Ar–H), 7.60-7.62 (m, 2H, Ar–H), 7.83-7.84 (m, 3H, Ar–H), 8.92 (s, 1H, NH), 10.04 (s, 1H, NH). ^{13}C NMR (DMSO-d_6): δ 20.78 (C-7″), 35.25 (C-9), 42.41 (C-8), 114.15 (C-3), 118.03 (C-2″, C-6″), 119.85 (C-1), 121.29 (C-5), 122.80 (C-2′, C-6′), 127.30 (C-3′, C-5′), 127.80 (C-6), 129.94 (C-3″, C-5″), 130.03 (C-4″), 133.72 (C-4), 133.94 (C-1″), 138.11 (C-4′), 145.04 (C-1′), 158.98 (C-2), 167.86 (C-7). HRMS (ESI$^+$): m/z [M + H]$^+$ calcd. for $C_{22}H_{21}ClN_2O_4S^+$ 444.9303 found 444.9311.

2.1.4.15. 5-Chloro-N-(4-(N-benzylsulfamoyl) phenethyl)salicylamide (34)

White crystals; yield 99%; mp 183–185 °C. ^{1}H NMR (400 MHz, DMSO-d_6): δ 2.92 (t, 2H, J = 13.31 Hz, CH_2), 3.77 (t, 2H, J = 13.32 Hz, CH_2), 3.92 (s, 2H, CH_2), 6.89-6.90 (m, 1H, Ar–H), 7.21 (d, 4H, J = 10 Hz, Ar–H), 7.38-7.41 (m, 3H, Ar–H), 7.90 (d, 3H, J = 10 Hz, Ar–H), 8.06 (s, 1H, Ar–H), 8.06 (s, 1H, NH), 8.91 (s, 1H, NH), 12.47 (s, 1H, OH). ^{13}C NMR (DMSO-d_6): δ 35.18 (C-9), 42.11 (C-8), 46.91 (C-7′), 118.13 (C-3), 119.83 (C-1), 122.90 (C-4″), 127.16 (C-5), 127.64 (C-2″, C-6″), 127.83 (C-2′, C-6′), 128.09 (C-3′, C-5′), 128.72 (C-5″), 129.09 (C-6), 129.95 (C-4), 133.75 (C-4′), 138.16 (C-1″), 144.55 (C-1′),158.92 (C-2), 167.91 (C-7). HRMS (ESI$^+$): m/z [M + H]$^+$ calcd. for $C_{22}H_{21}ClN_2O_4S^+$ 444.9303 found 444.9317.

2.1.4.16. 5-Chloro-N-(4-(N-phenethylsulfamoyl) phenethyl)salicylamide (35)

Brown crystals; yield 97%; mp 77–80 °C. ^{1}H NMR (400 MHz, DMSO-d_6): δ 2.64 (t, 2H, J = 12.60 Hz, CH_2), 2.91 (t, 2H, J = 12.60 Hz, CH_2), 3.41 (t, 2H, J =13.70 Hz, CH_2), 3.54 (t, 2H, J =13.70 Hz, CH_2), 6.89-6.90 (m, 1H, Ar–H),6.99- 7.20 (m, 3H, Ar–H), 7.22-7.24 (m, 2H, Ar–H), 7.40-7.42 (m, 2H, Ar–H), 7.86 (s, 1H, Ar–H), 8.92 (s, 1H, NH), 12.47 (s, 1H, OH). ^{13}C NMR (DMSO-d_6): δ 35.03 (C-8′), 35.82 (C-9), 42.11 (C-8), 44.58 (C-7′), 118.15 (C-3), 119.82 (C-1), 122.90 (C-4″), 126.73 (C-5), 127.19 (C-2″, C-6″), 127.80 (C-2′, C-6′), 128.82 (C-3′, C-5′), 129.15 (C-6), 129.97 (C-3″, C-5″), 133.73 (C-4), 138.93 (C-4′), 139.23 (C-1″), 144.58 (C-1′), 158.99 (C-2), 167.97 (C-7). HRMS (ESI$^+$): m/z [M + H]$^+$ calcd. for $C_{23}H_{23}ClN_2O_4S^+$ 458.9568 found 458.9561.

2.2. Biological evaluation

2.2.1. In vitro PD-L1 inhibition assay

The inhibitory activity of the compounds as PD-L1 inhibitors was determined using PD-1 [Biotinylated]: PD-L1 Inhibitor Screening ELISA Assay Pair (AcroBiosystems, USA) following the manufacturer's protocol. Briefly, the 96 wells in the plate were coated with human PD-L1 protein followed by applying 50 µM of the potential compounds to each well. Unblocked proteins were then bound to human PD-1-Biotin. Streptavidin-HRP followed by TMB was then added to each well and the ability of compounds to inhibit PD-1: PD-L1 binding was determined by comparing OD readings. The absorbance was obtained at 450 nm using a Synergy™ HTX Multi-Mode Microplate Reader (BioTek, Winooski, VT, USA).

2.2.2. Cytotoxicity assessment

The biological activity against breast cancer (MCF-7 and MDA-MB-231) and prostate cancer (DU-145 and PC-3) cell lines in comparison with fibroblasts as a normal cell line was screened using 10 µM and 100 µM concentrations. MCF-7, DU-145, and PC-3 cells were cultured in RPMI 1640 media (EuroClone S.p.A., Italy), while MDA-MB-231 and fibroblast were cultured in DMEM media (EuroClone S.p.A., Italy). All media were supplemented with 1% penicillin-streptomycin (EuroClone S.p.A., Italy), 1% L-Glutamine (EuroClone S.p.A., Italy), and 10% fetal bovine serum (FBS) (EuroClone S.p.A., Italy). Cells were incubated in a 37 °C incubator under a 5% CO_2 atmosphere. Treated and control cells were incubated for 72 hours to screen for their cellular toxicity. MTT (3-(4,5-dimethylthiazol-2-yl)-2,5-diphenyltetrazolium bromide) tetrazolium assay was carried out according to the manufacturer's protocol to detect the metabolic action of living cells using an MTT Cell Proliferation Assay (ATCC®30–1010K), the absorbance was then recorded at 570 nm using a Synergy™ HTX Multi-Mode Microplate Reader (BioTek, Winooski, VT, USA).

2.3. Virtual screening and Molecular docking

The X-ray diffraction pdb files 5j8o corresponding to the structure of human programmed cell death (hPD-L1) were downloaded from the protein data bank (www.rcsb.org/pdb/welcome.do) with resolution 2.30 and 2.30 A°, respectively. Their energy was minimized using the YASARA Energy Minimization Server (www.rcsb.org/pdb/welcome.do) and all water, bound ligands, and cofactors were removed. The conformers corresponding to each compound under investigation were created, energy minimized and saved as *pdb* file format using OSIRIS Datawarrior v5.5.0 (www.openmolecules.org). The pdbqt file format of the proteins and the compounds were created using MGL Tools 1.5.6 (www.mgltools.scripps. edu). Docking calculation was performed using Auto Dock Vena [49] and PyRx 0.8 (www.mgltools.scripps.edu). The results were analyzed based on the binding affinity of the ligand at the inhibitory pocket and hydrogen bonding formed using BIOVA Studio Visualizer v21.1.0.20298 (www.3dsbiova.com).

3. Results and Discussion

3.1. Virtual screening

3.1.1. Database

One of the most important computational techniques recently used in drug discovery is virtual screening. It is used to identify the structures, which are most likely to bind with drug targets such as protein receptors or enzymes. Recently, several high-resolution crystal structures establishing the structural foundations of human PD-1 (hPD-1) and PD-L1 (hPD-L1) were published and available in the protein data bank [15]. The obtained crystals provide important information about the hPD-1/hPD-L1 interaction and the details of the binding modes.

Unlike the traditional approaches to drug discovery, which rely on a step-wise synthesis and screening of large numbers of compounds to optimize activity profiles, scientists have used computer models of new chemical entities to help define the activity profiles, geometries, and reactivity of the target compounds. Furthermore, in medicinal chemistry, biological activity is dependent on the three-dimensional positioning of the pharmacophore. So, the improvement of new mathematical models that describe chemical phenomena and the development of more program interfaces coupled with the availability of high-technology computer hardware has provided scientists with a new set of computational tools. To rationalize the prospected biological activity and to describe the binding mode of the active compounds with their predicted intracellular target, docking analysis should be carried out.

In the present study, virtual screening of the self-database of some sulfonamide derivatives as inhibitors for the PD-1/PD-L1 pathway was created first, followed by synthesis and determination of its bioactivity. The self-database of the sulfonamide derivatives was designed with the assistance of different molecular modeling and drug discovery computer programs. This creation was made with the understanding that protein inhibitors should have small molecular sizes that fit in the inhibitory pocket containing hydroxyl, amino, or oxo groups to form hydrogen bonds and an aryl group to allow for hydrophobic interaction. Additionally, the flexibility of the inhibitors was improved by gradually increasing the number of internal single bonds (Fig. 1).

The 2D structure corresponding to each compound was drawn and saved in sck file format using BIOVA Draw v21.1.NET. It was converted to a 3D structure and saved as *mol* file format using BIOVA Studio Visualizer v21.1.0.20298 (www.3dsbiova.com). The structure in *mol* file format was energy minimized and saved as *pdb* file format using the VEGA ZZ program (Drug Design Laboratory website). The conformers corresponding to each compound were created, energy minimized and saved as *pdb* file format using OSIRIS Datawarrior v5.5.0 (www.openmolecules.org).

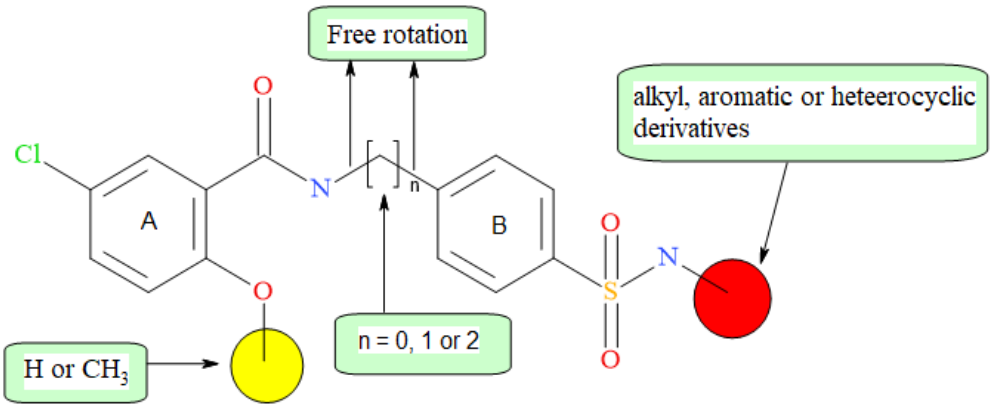

Fig. 1. The structure of the sulfonamides database used in the virtual screening.

3.1.2. Target Protein

PD-L1 is a type I transmembrane protein and the PD-1/PD-L1 interaction releases a co-inhibitory signal to activated T cells, which induces T cell apoptosis, energy, and functional exhaustion. As a result, T cells' activities to antigenic stimuli including proliferation, cytokine secretion, and cytolytic activity are reduced. Normally, PD-1 and widely expressed PD-L1 act as an intrinsic negative feedback system to down-regulate the immune system and promote self-tolerance by suppressing T cell inflammatory activity. However, the over-expressed PD-L1 on the surface of tumor cells can induce T-cell dysfunction and suppress antigen-specific T-cell responses [15].

The crystal structure of human programmed cell death (hPD-L1, 5g8o) that has been solved by X-ray crystallography was downloaded from the Protein Data Bank website (www.rcsb.org) as a *pdb* file format. Its structure was corrected and energy was minimized using the YASARA Energy Minimization Server (www.rcsb.org/pdb/welcome.do). All ligands and cofactors were removed and prepared for virtual screening in *pdbqt* file format using the MGL Tools Program (www.mgltools.scripps.edu).

The inhibitory pocket of the target protein was analyzed and the amino acid chains that surround the native ligand were defined. It composed of Chain A (ILE54, VAL55, TYR56, ASN63, GLN66, VAL68, VAL76, MET115, ILE116, SER117, ALA121, ASP122, TYR123) and chain B (PHE19, ILE54, VAL55, TYR56, MET115, ILE116, SER117, ALA121, ASP122, TYR123, LYS124). The native ligand and the surrounding amino acids are illustrated in Fig. 2.

3.1.3. Docking calculation and Results analysis

The sulfonamide database created was docked into the inhibitory pocket of the hPD-L1 binding site to deduce the binding affinity (kcal/mol) using AutoDock Vena and PyRx programs (www.mgltools.scripps.edu). The binding affinity is used to describe the affinity between a ligand (such as a drug) and a protein, i.e. how tightly a ligand binds to a particular protein. Ligand-protein affinities (kcal/mol) are influenced by non-covalent intermolecular interactions such as hydrogen bonding, electrostatic interactions, hydrophobic and Van der Waals forces. The result analysis was performed using BIOVA Studio Visualizer v21.1.0.20298 (www.3dsbiova.com). By taking into consideration the binding affinity of the native ligand (6GZ), compounds with binding affinity as low as -9.5 kcal/mol are considered promising compounds, and subjected to synthesis and testing directly against the target protein. Table 1 illustrates the promising compounds, their binding affinity, and the hydrogen bonds formed.

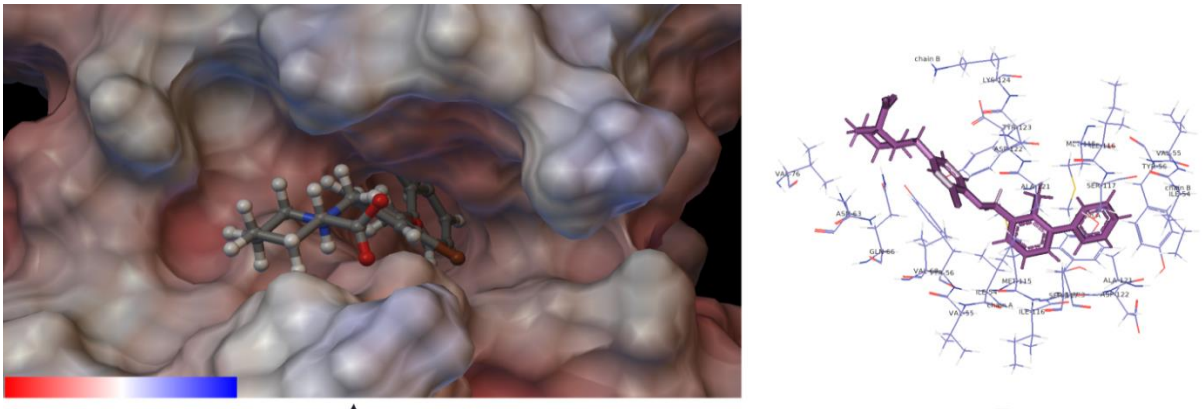

A B

Fig. 2. A. The inhibitory pocket of the hPD-L1 (PDB ID: 5j8o). The outermost surface of the enzyme was illustrated as an electrostatic potential map and the native inhibitor as a gray ball and stick; B. The amino acids surrounding the inhibitory pocket are illustrated as lines and the native ligand is a pink ball and stick.

3.2. Chemistry

Based on the analysis of the docking results, the promising compounds were synthesized using the organic chemistry methods that we had previously published (Scheme 1) [42-48].

In series 1, the amidation of 5-chloro-*o*- anisic acid with benzylamine was performed using a mixed anhydride method to afford 5-chloro-2-methoxy-N-benzylbenzamide [47]. In series 2, benzyl amine was replaced with beta-phenethylamine to increase the flexibility of the produced compound by increasing the possible rotation around the single bonds. The benzamides formed were treated with chlorosulfonic acid in an ice bath for 24 hours to yield the corresponding benzenesulfonyl chloride derivatives.

Table 1. Compounds were selected for synthesis and testing as hPD-L1 inhibitors according to the virtual screening and formed hydrogen bonds with the amino acid residues.

Compounds	*pdb ID: 5j8o			Compounds	*pdb ID: 5j8o		
	**B.A.	Chain A amino	Chain B amino acids		**B.A.	Chain A amino acids	Chain B amino acids
4	-9.8	-	ALA121	**5**	-10.2	-	ALA121
6	-9.8	-	ALA121	**7**	-10.1	-	ALA121
8	-9.3	GLN66	PHE19	**9**	-10.3	MET115	-
10	-9.8	GLN66	PHE19	**11**	-9.5	GLN66	PHE19
12	-9.5	GLN66	-	**13**	-9.8	-	ASP122
14	-9.8	GLN66	PHE19	**15**	-10.3	GLN66	LYS124
16	-9.6	GLN66	-	**17**	-9.7	-	PHE19
18	-9.5	GLN66	PHE19	**19**	-9.7	GLN66	PHE19
20	-10.1	-	ALA121, ASP122	**21**	-10.0	-	ALA121, ASP122
22	-10.0	GLN66	ASP122	**23**	-10.1	-	ASP122
24	-9.6	MET115	PHE19	**25**	-10.4	-	PHE19
26	-10.4	ILE116, ASP122	-	**27**	-10.0	GLN66	PHE19
28	-10.4	ILE116	-	**29**	-10.6	GLN66, ILE116, ASP122	-
30	-10.6	GLN66	ALA121	**31**	-10.5	GLN66, MET115	PHE19, ALA121
32	-9.6	-	PHE19	**33**	-10.4	ILE116	-
34	-9.9	ILE116, ASP122	-	**35**	-10.0	GLN66	PHE19, ALA121
***NL 6GZ	-11.5	GLN 66	-				

*X-ray diffraction of human programmed cell death 1, ** Binding Affinity, kcal/mole and ***Native ligand

Using the reported method [42], benzenesulfonyl chloride derivatives were coupled with appropriate aromatic amines in the presence of sodium carbonate in a mixture of dichloromethane (DCM) and water (2:1 in ratio) to yield benzamide derivatives **4**–**19**. Finally, by refluxing the appropriate benzamide derivatives (**4**–**19**) with KCN in anhydrous DMSO, the methoxy group can be demethylated with a hydroxyl group to give the corresponding salicylamides **20**–**35** [42]. The structure of the synthesized compounds was established by the use of spectroscopic tools such as ^{1}H NMR, ^{13}C NMR, and high-resolution mass spectra.

3.3. Biological evaluation

3.3.1. In vitro PD-L1 inhibition assay

Immune checkpoint signaling pathways are the focus of contemporary cancer research. PD-1 is one of the best-characterized checkpoint proteins. The binding between PD-1 and its ligand PD-L1 inhibits T-cell activation and allows cancer cells to evade the body's immune surveillance. Thus, pharmacological inhibition of PD-1 or its ligands has been considered a promising strategy by many oncologists [50].

The PD-1 [Biotinylated]: PD-L1 inhibitor screening enzyme-linked immunosorbent assay (ELISA) Kit is designed to facilitate the identification and characterization of novel inhibitors of the PD-1 pathway. The assay utilizes the binding of biotinylated human PD-1 to immobilized human PD-L1 in a functional ELISA assay using a simple colorimetric sandwich ELISA platform. The experiment consists of 4 easy steps: a) overlaid the plate with human PD-L1.

b) Added the potential compounds corresponding to 50 μM to the test.

c) Added human PD-1 biotin to bind coated human PD-L1.

d) Added Streptavidin-HRP followed by 3,3',5,5'-Tetramethylbenzidine (TMB) or other Horseradish Peroxidase (HRP) colorimetric substrate.

Finally, the ability of potential compounds to inhibit PD-1: PD-L1 binding is determined by comparing optical density (OD) readings between different experimental groups. Table 2 illustrates the results of the inhibitory screening in order from the most active to the least active.

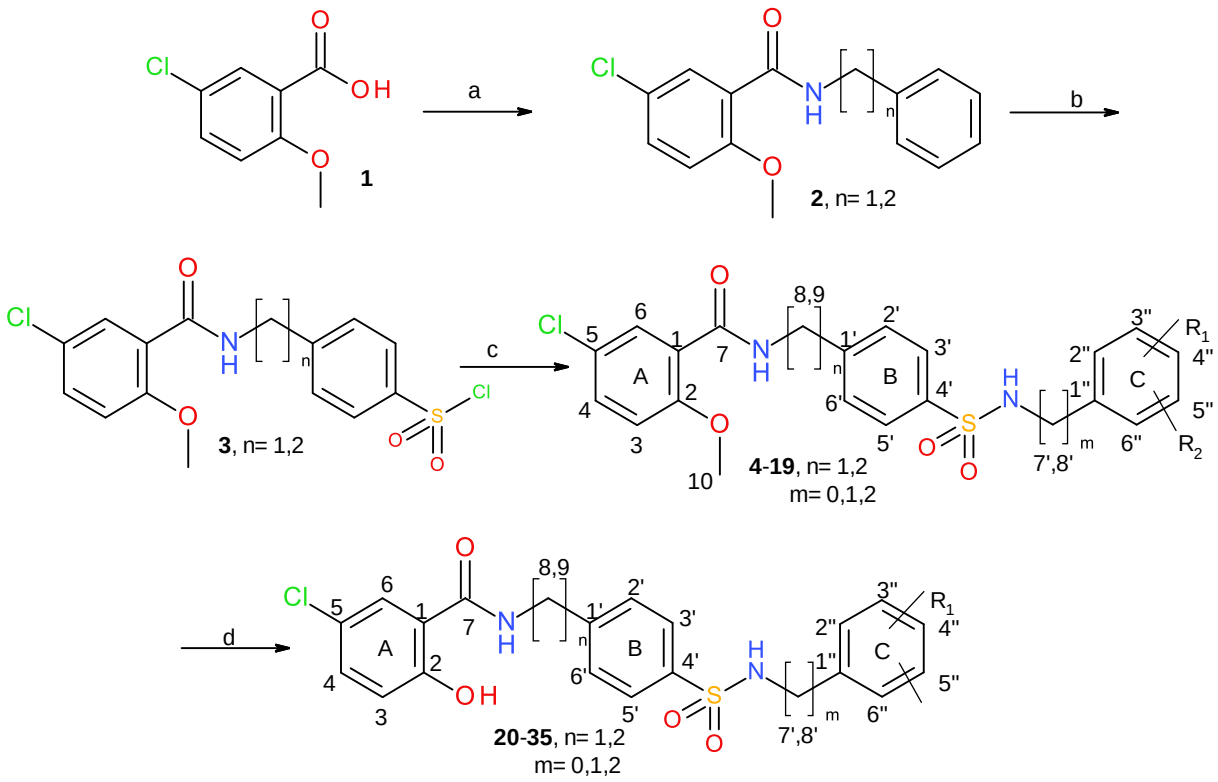

4,20: n = 1, R_1 = 4"-F, R_2 = H, m = 0
5,21: n = 1, R_1 = 2"-F, R_2 = H, m = 0
6,22: n = 1, R_1 = 3"-F, R_2 = H, m = 0
7,23: n = 1, R_1 = 2"-F, R_2 = 4"-F, m = 0
8,24: n = 1, R_1 = 3"-CF_3, R_2 = H, m = 0
9,25: n = 1, R_1 = 4"-CF_3, R_2 = H, m = 0
10,26: n = 2, R_1 = 4"-Cl, R_2 = H, m = 0
11,27: n = 2, R_1 = H, R_2 = H, m = 0
12,28: n = 2, R_1 = 4"-F, R_2 = H, m = 0
13,29: n = 2, R_1 = 2"-F, R_2 = H, m = 0
14,30: n = 2, R_1 = 3"-F, R_2 = H, m = 0
15,31: n = 2, R_1 = 4"-CF_3, R_2 = H, m = 0
16,32: n = 2, R_1 = 4"-Br, R_2 = H, m = 0
17,33: n = 2, R_1 = 4"-CH_3, R_2 = H, m = 0
18,34: n = 2, R_1 = H, R_2 = H, m = 1
19,35: n = 2, R_1 = H, R_2 = H, m = 2

Scheme 1. Synthesis of compounds has binding affinity as low as -9.5 kcal/mol and was considered the basic criteria for further study. Reagents and conditions: a) ethyl chloroformate, triethylamine, benzylamine and/or beta-phenethylamine, DCM, RT, 2 h; b) chlorosulfonic acid, RT, overnight; c) appropriate amine, sodium carbonate, DCM/H2O (2:1), RT, 24h; d) potassium cyanide, DMSO, reflux, 1 h.

Table 2. The inhibitory activity percentage of the potential compounds (50 µM) in order according to the most active to the least active.

Compounds	% Inhibition	Compounds	% Inhibition	Compounds	% Inhibition	Compounds	% Inhibition
30	57.152	**4**	53.327	**17**	51.253	**31**	51.058
7	50.993	**5**	48.984	**28**	48.854	**9**	46.326
6	43.928	**27**	43.928	**13**	42.307	**21**	42.242
35	41.789	**26**	41.724	**33**	41.465	**22**	40.687
18	39.714	**29**	37.510	**8**	36.992	**15**	33.815
25	32.584	**10**	32.065	**20**	31.676	**11**	29.991
24	29.602	**19**	29.472	**16**	28.370	**14**	27.982
23	26.16681	**32**	24.93518	**12**	24.1573	**34**	12.4892

In the present study, five compounds (**4**, **7**, **17**, **30**, and **31**) have the ability to inhibit PD-L1 with more than 50%. Four of them have fluorine atoms in ring C, while the 5th (**17**) has a methyl group in the *para*

position in ring C. The most active compound **30** with 57.152% inhibition has a fluorine atom in *m*-position in addition to a hydroxyl group in ring A, while compound **7** with 50.993% has *o*- and *p*-fluorine atoms in ring C and methoxyl group in ring A.

Based on the results obtained from the *in vitro* testing of the PD-L1 inhibition and to understand the relation between the structure of the active compounds **4**, **7**, **17**, **30**, and **31** and their activities, their binding mode in the hotspot of the crystal structure of human programmed cell death (hPD-L1, PDB ID: 5g8o) was analyzed in details (Figs. 3-7). The native ligand (6GZ) was used as a reference compound, which formed a strong hydrogen bond (bond length 2.12 Aº) with A; GLN66. Based on the analysis conducted, it was found that the polar moieties salicylamide or anisamide played a crucial role in forming hydrogen bonds with the amino acids in the hotspot region of the protein. The *keto* group of the amide group of compounds **30** and **31** (Figs. 6 and 7) formed strong hydrogen bonds (2.78 and 2.60 Aº, respectively) with A; GLN66, while the proton of the amide group of compounds **4**, **7**, **30** and **31** (Figs. 3, 4, 6 and 7) formed strong hydrogen bonds (2.29, 2.25, 2.22 and 2.25 Aº, respectively) with B: ALA121. Also, the oxygen in ring A of compounds **17** and **31** (Figs. 5 and 7) formed strong hydrogen bonds (2.31 and 2.31 Aº, respectively) with B: PHE19. The role of the fluorine atoms in increasing the potency of the compounds **4**, **7**, **30**, and **31** are reflected in the polar contact found with the amino acids A: ALA121 and B: ILE54, VAL55, MET115, ILE116, ASP122 (Figs. 3-7).

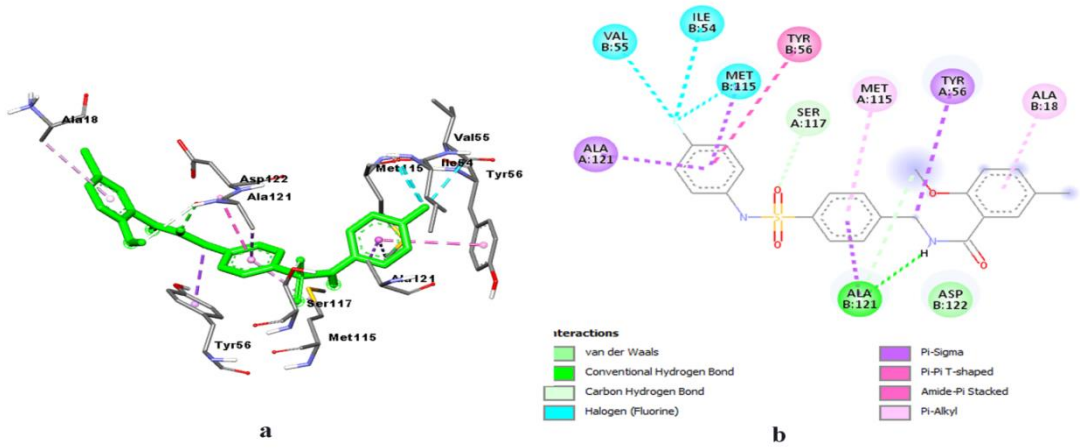

Fig. 3. 3D (**a**) and 2D (**b**) binding mode of compound **4** (colored according to the functional groups) docked into the hotspot of human Programmed cell death 1 (PDB ID: 5j8o). The rest of the enzyme structure was deleted from the view to clarify the docked conformer. The green dashed lines indicate hydrogen bonds with B: ALA121. The blue dashed lines showed the polar contact of the fluorine atom with B: ILE54, VAL55, and MET115. The pink and red dashed lines showed pi-sigma and pi-pi stacked interaction, respectively. The pall red dashed lines illustrated the hydrophobic interaction with A: MET115, and B: ALA18.

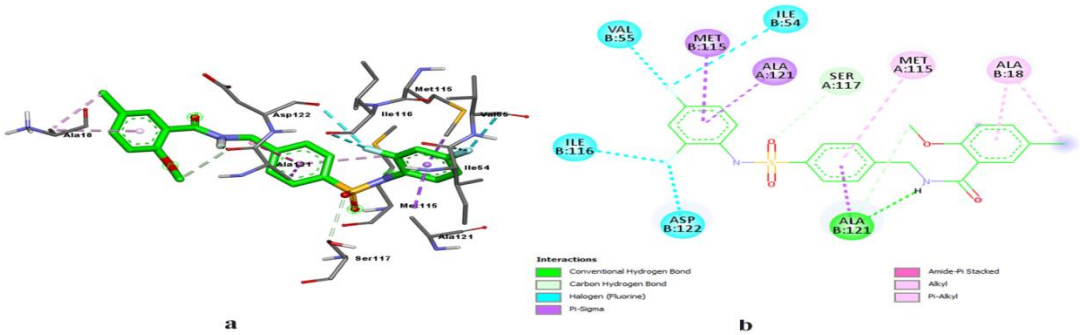

Fig. 4. 3D (**a**) and 2D (**b**) binding mode of compound **7** (colored according to the functional groups) docked into the hotspot of human programmed cell death 1 (PDB ID: 5j8o). The rest of the enzyme structure was deleted from the view to clarify the docked conformer. The green dashed lines indicate hydrogen bonds with B: ALA121. The blue dashed lines showed the polar contact of the fluorine atom with B: ILE54, VAL55, ILE116, and ASP122. The pink dashed lines showed pi-sigma interaction. The pall red dashed lines illustrated the hydrophobic interaction with A: MRT115 and B: ALA18.

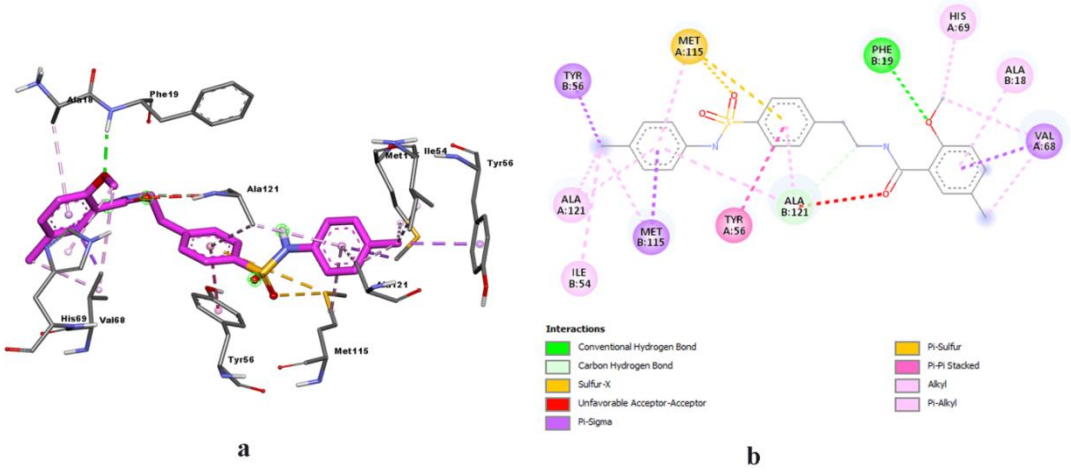

Fig. 5. 3D (a) and 2D (b) binding mode of compound **17** (colored according to the functional groups) docked into the hotspot of human programmed cell death 1 (PDB ID: 5j8o). The rest of the enzyme structure was deleted from the view to clarify the docked conformer. The green dashed lines indicate hydrogen bonds with B: PHE19. The pink and red dashed lines showed pi-sigma and pi-pi stacked interaction, respectively. The pall red dashed lines illustrated the hydrophobic interaction with A: HIS69, ALA121, and B: ALA18, ILE54. The yellow dashed lines showed pi-sulfur interaction with MET115.

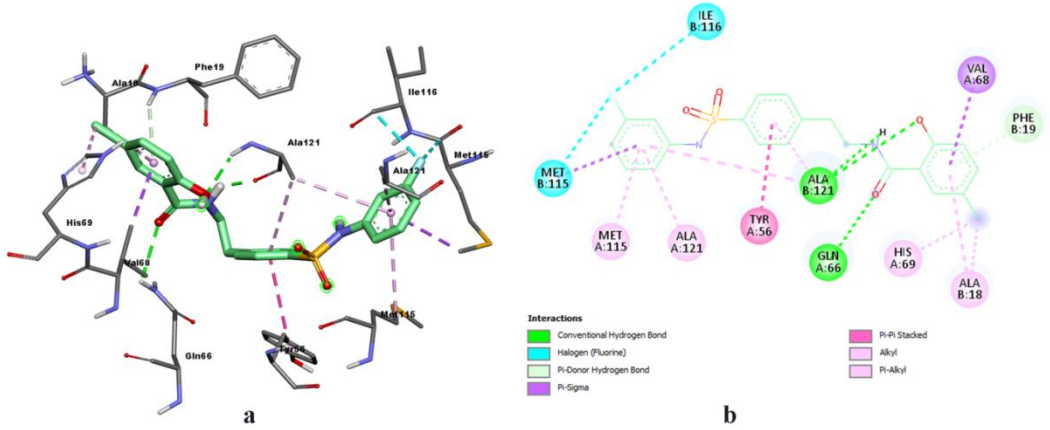

Fig. 6. 3D (a) and 2D (b) binding mode of compound **30** (colored according to the functional groups) docked into the hotspot of human programmed cell death 1 (PDB ID: 5j8o). The rest of the enzyme structure was deleted from the view to clarify the docked conformer. The green dashed lines indicate hydrogen bonds with A: GLN66 and B: ALA121. The blue dashed lines showed the polar contact of the fluorine atom with B: MET115 and B: ILE116. The pink and red dashed lines showed pi-sigma and pi-pi stacked interaction, respectively. The pall red dashed lines illustrated the hydrophobic interaction with A: HIS69, ALA112, MET115, and B: ALA18.

3.3.2. In vitro anti-proliferative activity and cytotoxicity effect

Within the framework of our efforts exerted in the evaluation of the sulfonamide derivatives coupled with salicylamide or anisamide scaffold [42-48], in vitro anti-proliferative activity against four types of human cell lines was tested at 10 μM. The objective of this study is to evaluate the safety of PD-L1 active compounds and compare their anti-proliferative activity with that of other compounds under investigation. The compounds were tested against human breast cancer cell lines MCF-7 which have estrogen, progesterone, and glucocorticoid receptors [51]. Also, two human prostate cancer cell lines DU-145 and PC-3 were considered to be the standard prostate cancer cell lines used in therapeutic research and drug development [51-53]. The second cell line did not respond to androgens, glucocorticoid, or fibroblast growth factors, but it was influenced by epidermal growth factors. Fibroblast was used in the present study as a normal cell line and it is a type of biological cell that synthesizes the extracellular

matrix and collages, producing the structural framework role in wound healing [54]. The results of the anti-proliferative activity and their cytotoxic effect on the fibroblast cell line are illustrated in Table 3.

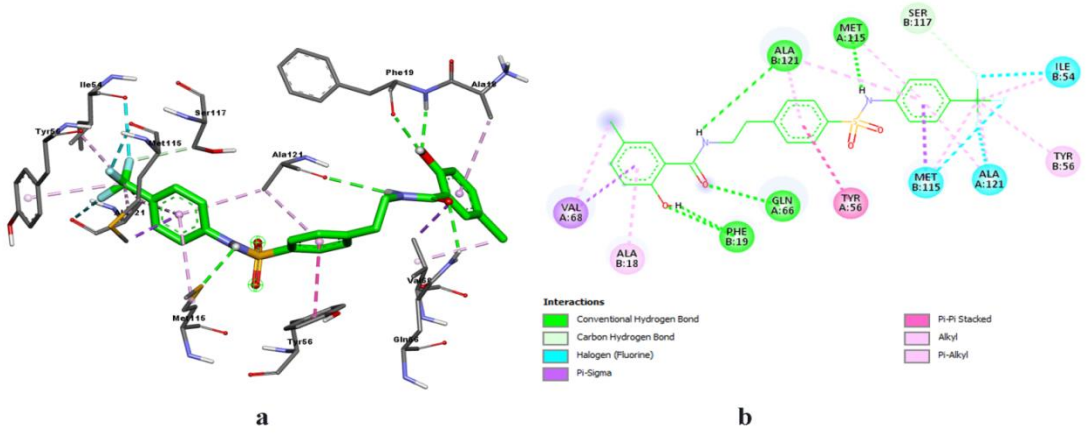

Fig. 7. 3D (a) and 2D (b) binding mode of compound **31** (colored according to the functional groups) docked into the hotspot of human Programmed cell death 1 (PDB ID: 5j8o). The rest of the enzyme structure was deleted from the view to clarify the docked conformer. The green dashed lines indicate hydrogen bonds with A: GLN66, MET115, and B: PHE19, ALA121. The blue dashed lines showed the polar contact of the fluorine atom with A: ALA121 and B: ILE54, MET115. The pink and red dashed lines showed pi-sigma and pi-pi stacked interaction, respectively. The pall red dashed lines illustrated the hydrophobic interaction with B: ALA18 and TYR56.

The compounds that have inhibitory activity against PD-L1 (**4, 7, 17, 30,** and **31**) were found to be safe and did not have any cytotoxic effects on the fibroblast cell lines. Moreover, compounds **4, 7, 17,** and **30** showed little to no anti-proliferative activity against the cell lines used in this study except compound **4**, which displayed anti-proliferative activity against PC-3 (66.640%). On the other hand, compound **31** showed remarkable activities against the cell lines MCF7, DU-145, and PC-3 with 67.756%, 44.403%, and 64.737% respectively. Overall, the human prostate cancer cell line PC-3 is highly sensitive toward the tested compounds as compound **23** is the most active with 83.760%, and compounds **4, 19, 22, 24, 29, 31,** and **33** display anti-proliferative activity with more than 50%.

Table 3*. Percentage of the antiproliferative activity of the compounds under investigation against the tested human cancer cell lines and their cytotoxic effect on fibroblast cell lines at 10 µM.

Compounds	MCF-7	DU-145	PC-3	Fibroblast
4	2.203	6.473	66.640	-2.004
5	-46.137	-0.714	-11.798	2.920
6	-13.059	13.295	7.168	36.855
7	-11.389	-0.024	-11.598	-23.682
8	-17.745	11.509	-7.056	3.493
9	-26.513	15.204	18.121	-1.947
10	5.219	25.560	24.465	12.772
11	24.2867	8.463	0.890	7.531
12	7.817	1.437	24.766	20.360
13	0	0	0	0
14	-0.162	28.037	-18.143	-16.093
15	7.167	20.524	-8.993	-17.898
16	-7.306	17.357	-15.004	7.388
17	7.956	15.367	-13.869	-1.145
18	17.374	18.372	2.593	-16.036
19	19.879	27.063	55.253	5.698

20	-13.430	11.793	39.058	17.182
21	36.720	17.154	34.283	8.161
22	-11.853	7.123	53.784	6.729
23	11.111	3.955	83.670	8.676
24	19.693	22.636	55.487	15.206
25	11.899	9.884	40.360	-5.870
26	0	0	0	0
27	0	0	0	0
28	0	0	0	0
29	24.054	21.946	49.643	-5.011
30	0	0	0	0
31	67.756	44.403	64.737	4.495
32	0	0	0	0
33	16.214	24.788	56.890	5.441
34	0	0	0	0
35	0	0	0	0

*Positive results showed anti-proliferative activities, while negative results showed proliferative activities.

3.3.3. In silico ADMET prediction

In silico physicochemical properties, lipophilicity, solubility, absorption, distribution, metabolism, and toxicity parameters of compounds **4**, **7**, **17**, **30**, and **31** are predicted using the admetSAR website [55] and are summarized in Table 4. The promising compound selected is found to be favorable in an acceptable prediction.

Table 4. *In silico* ADMET predictions of the selected active compounds as a PD-L1 inhibitor

Compounds	**4**	**7**	**17**	**30**	**31**
Physicochemical properties					
Molecular weight	448.90	466.891	458.965	448.901	498.908
clogP[1]	4.22	4.36	4.1256	3.6068	4.3543
clogS	-5.135	-5.659	-5.487	-5.143	-5.607
H acceptors	6	6	6	6	6
H donor	2	2	2	3	3
Topological polar surface	92.88	92.88	92.88	103.88	103.88
Rotatable bonds	7	7	8	7	7
Absorption					
Human Intestinal Absorption (HIA)	+	+	+	+	+
Human oral bioavailability (HOB)	+	+	+	+	+
Caco-2 permeability	-	-	-	-	-
Distribution					
Plasma protein binding	1.017	0.921	0.906	0.954	0.968
P-glycoprotein inhibitor	+	+	+	+	+
P-glycoprotein substrate	-	+	+	+	+
Blood Brain Barrier	-	-	+	+	+
Metabolism					

CYP1A2 inhibition	-	-	-	-	-
CYP2C19 inhibition	+	+	+	-	-
CYP2C9 inhibition	+	+	+	+	+
CYP2C9 substrate	-	-	-	-	-
CYP2D6 inhibition	-	-	+	+	+
CYP2D6 substrate	-	-	-	-	-
CYP3A4 inhibition	+	+	+	-	-
CYP3A4 substrate	+	+	+	+	+
CYP inhibitory promiscuity	+	+	+	+	+
BRCP inhibitor	-	-	-	-	-
BSEP inhibitor	+	+	+	+	+
OATP1B1 inhibitor	+	+	+	+	+
OATP1B3 inhibitor	+	+	+	+	+
OATP2B1 inhibitor	-	-	-	-	-
OCT1 inhibitor	-	-	-	-	-
OCT2 inhibitor	-	-	-	-	-
MATE1 inhibitor	-	-	-	-	-
Toxicity					
Hepatotoxicity	+	+	+	+	+
Human Ether-a-go-go-Related Gene inhibition	+	+	+	-	+
Acute Oral Toxicity (c)	III[2]	III[2]	III[2]	III[2]	III[2]
Eye corrosion	-	-	-	-	-
Eye irritation	-	-	-	-	-
Ames mutagenesis	-	-	-	-	-
Crustacean aquatic	-	-	-	-	-
Carcinogenicity (binary)	+	+	-	-	-
Mitochondrial toxicity	+	+	+	+	+
Micronuclear	+	+	+	+	+
Nephrotoxicity	+	+	-	-	-
Acute Oral Toxicity[3]	1.809	2.086	1.308	1.913	1.933
Reproductive toxicity	-	-	-	-	-
Respiratory toxicity	+	+	+	+	+
skin sensitization	-	-	-	-	-
Other Important ADMET					
Androgen receptor	-	-	-	-	+
Aromatase binding	-	-	-	+	+
Estrogen receptor	+	+	-	-	+
Glucocorticoid receptor binding	+	+	+	-	+
PPAR gamma	+	+	+	+	+
Subcellular localization	Mitochondria	Mitochondria	Mitochondria	Mitochondria	Mitochondria
Thyroid receptor binding	+	+	+	+	+
UGT catalysed	-	-	-	+	+

[1] Average of five method predictions (iLOGP, XLOGP, WLOGP3, MLOGP, and SILICO-IT).
[2] III = LD50 > 500 < 5000 mg/kg
[3] log(1/(mol/kg))

4. Conclusions

Based on *in silico* virtual screening of sulfonamides self-database against immune checkpoint PD-L1, 32 sulfonamide derivatives coupled with salicylamide or anisamide scaffold were synthesized and tested *in vitro* as PD-L1 inhibitor using screening ELISA assay. Five compounds (**30**, **4**, **17**, **31**, **7**) gave promising results with more than 50% inhibition. All compounds were found to be safe and have no cytotoxic effect against the fibroblast cell lines. Moreover, compounds **4**, **7**, **17,** and **30** showed little to no anti-proliferative activity against the cell lines used in this study except compound **4**, which displayed anti-proliferative activity against PC-3. On the other hand, compound **31** showed remarkable activities against the cell lines MCF-7, DU-145, and PC-3. Overall, the human prostate cancer cell line PC-3 is highly sensitive
toward some of the 32 compounds tested at 10 μM. The results of this study indicate a new class of safe sulfonamide derivatives as PD-L1 inhibitors, which can be developed to increase their activity against immune checkpoint PD-L1.

5. Conflicts of interest

The authors declare that they have no competing interests.

6. Formatting of funding sources

The study was supported by the Pharmaceutical and Drug Industries Research Institute, National Research Centre, Egypt under Grant (Number 12060114).

7. Acknowledgments

The authors thank their colleagues at the National Research Centre, Egypt, Al-Zaytoonah University, Jordan, and Al-Balqa Applied University, Jordan for their support.

8. References

[1] Kedmi M, Avigdor A, Nagler A. Anti-PD-1-targeted therapies focusing on lymphatic malignancies: biological rationale, clinical challenges and opportunities. Acta Haematol. 2015;133:129-135. https://doi.org/10.1159/000362151

[2] Tsirigotis P, Savani BN, Nagler A. Programmed death-1 immune checkpoint blockade in the treatment of hematological malignancies. Ann Med. 2016;48(6):428-439. https://doi.org/10.1080/07853890.2016.1186827

[3] Boussiotis VA, Chatterjee P, Li L. Biochemical signaling of PD-1 on T cells and its functional implications. Cancer J. 2014;20(4):265-71. https://doi.org/10.1097/ppo.0000000000000059

[4] Gunturi A, McDermott DF. Nivolumab for the treatment of cancer. Expert Opin Investig Drugs. 2015;4(2):253-60. https://doi.org/10.1517/13543784.2015.991819

[5] McDermott DF, Atkins MB. PD-1 as a potential target in cancer therapy. Cancer Med. 2013;2(5):662-73. https://doi.org/10.1002%2Fcam4.106

[6] Gunturi A, McDermott DF. Potential of new therapies like anti-PD1 in kidney cancer. Curr Treat Options Oncol. 2014;15(1):137-46. https://doi.org/10.1007/s11864-013-0268-y

[7] Murakami N, Riella LV. Co-inhibitory pathways and their importance in immune regulation. Transplantation 2014;98(1):3-14. https://doi.org/10.1097/tp.0000000000000169

[8] Weinstock M, McDermott D. Targeting PD-1/PD-L1 in the treatment of metastatic renal cell carcinoma. Ther Adv Urol. 2015;7(6):365-77. https://doi.org/10.1177%2F1756287215597647

[9] Zhang J, Dang F, Ren J, Wei W. Biochemical Aspects of PD-L1 Regulation in Cancer Immunotherapy Trends Biochem Sci. 2018;43(12):1014-1032. https://doi.org/10.1016%2Fj.tibs.2018.09.004

[10] Mahoney KM, Freeman GJ, McDermott DF. The Next Immune-Checkpoint Inhibitors: PD-1/PD-L1 Blockade in Melanoma. Clin Ther. 2015;37(4):764-82. https://doi.org/10.1016%2Fj.clinthera.2015.02.018

[11] Bardhan K, Anagnostou T, Boussiotis VA. The PD1: PD-L1/2 Pathway from Discovery to Clinical Implementation. Front Immunol. 2016;7:550. https://doi.org/10.3389%2Ffimmu.2016.00550

[12] Nishijima TF, Shachar SS, Nyrop KA, Muss HB. Safety and Tolerability of PD-1/PD-L1 Inhibitors Compared with Chemotherapy in Patients with Advanced Cancer: A Meta-Analysis. Oncologist. 2017;22(4):470-479. https://doi.org/10.1634/theoncologist.2016-0419

[13] Shen X, Zhang L, Li J, Li Y, Wang Y, Xu ZX. Recent Findings in the Regulation of Programmed Death Ligand 1 Expression. Front Immunol. 2019;10:1337. https://doi.org/10.3389/fimmu.2019.01337

[14] Differding, "AUNP-12-A Novel Peptide Therapeutic Targeting PD-1 Immune Checkpoint Pathway for Cancer Immunotherapy-Structure Activity Relationships & Peptide/Peptidomimetic Analogs," available at http://www.differding.com/data/AUNP_12_A_novel_peptide_therapeutic_targeting_PD_1_immune_checkpoint_pathwayfor_cancer_immunotherapy.pdf, Feb. 26, 2014

[15] Chen T, Li Q, Liu Z, Chen Y, Feng F, Sun H. Peptide-based and small synthetic molecule inhibitors on PDAss-1/PD-L1 pathway: A new choice for immunotherapy?. European Journal of Medicinal Chemistry 2019;161:378-398. https://doi.org/10.1016/j.ejmech.2018.10.044

[16] Chupak LS, Zheng X. Compounds Useful as Immunomodulators. 2015;WO2015034820 A1.

[17] Acúrcio RC, Pozzi S, Carreira B, et al. Therapeutic targeting of PD-1/PD-L1 blockade by novel small molecule inhibitors recruits cytotoxic T cells into solid tumor microenvironment. Journal for ImmunoTherapy of Cancer 2022; doi:10.1136/ jitc-2022-004695.

[18] Drews J. Drug Discovery: A Historical Perspective. Science 2000;287:1960–1964.

[19] Stokes SS, Albert R, Buurman ET, Andrews B, Shapiro AB, Green OM, McKenzie AR, Otterbein LR. Inhibitors of the acetyltransferase domain of N-acetylglucosamine-1-phosphate-uridylyltransferase/glucosamine-1-phosphate-acetyltransferase (GlmU). Part 2: Optimization of physical properties leading to antibacterial aryl sulfonamides. Bioorg & Med Chem Lett. 2012;22:7019–7023.

[20] Ajeet A, Tripathi L, Kumar A. Synthesis, Spectral Characterization, Docking Studies and QSAR Screening of 4-amino-benzenesulfonamides/N-acetyl 4-amino-benzenesulfonamide Derivatives as Antimicrobial Agents. J Pharm Nutr Sci. 2014;4:135–153.

[21] Ezabadi IR, Camoutsis C, Zoumpoulakis P, Geronikaki A, Soković M, Glamočilija J, Čirič A. Sulfonamide-1,2,4-triazole derivatives as antifungal and antibacterial agents: synthesis, biological evaluation, lipophilicity, and conformational studies. Bioorg Med Chem. 2008;16:1150–1161.

[22] Kennedy JF, Thorley M. Pharmaceutical Substances, 3rd Ed, A. Kleeman, J. Engel, B. Kutscher & D. Reichert George Thieme Verlag, Stuttgart/New York, 1999:2286 pp., ISBN 3-13-558403-8 / 0-86577-817-5.[0pt] [Electronic Version. ISBN 3-13-115133-1 / 0-86577-818-3]. Bioseparation 1999;8:336.

[23] Supuran CT, Casini A, Scozzafava A. Protease inhibitors of the sulfonamide type: Anticancer, antiinflammatory, and antiviral agents. Med Res Rev. 2003;23:535–558.

[24] Ogden RC, Flexner CW. Protease Inhibitors in AIDS Therapy. ed M Dekker, New York, Basel. 2001:27–48.

[25] Domagala JM, Bader JP, Gogliotti RD, Sanchez JP, Stier MA, Song Y, et al. A new class of anti-HIV-1 agents targeted toward the nucleocapsid protein NCp7: the 2,2'-dithiobisbenzamides. Bioorg Med Chem. 1997;5:569–579.

[26] Yoshino H, Ueda N, Niijima J, Sugumi H, Kotake Y, Koyanagi N, Yoshimatsu K, Asada M, et al. Novel sulfonamides as potential, systemically active antitumor agents. J Med Chem. 1992;35:2496–2497.

[27] Ma T, Fuld AD, Rigas JR, Hagey AE, Gordon GB, Dmitrovsky E, Dragnev KH. A Phase I Trial and in vitro Studies Combining ABT-751 with Carboplatin in Previously Treated Non-Small Cell Lung Cancer Patients. Chemotherapy. 2012;58:321–329.

[28] Mohan R, Banerjee M, Ray A, Manna T, Wilson L, Owa T, Bhattacharyya B, Panda D. Antimitotic sulfonamides inhibit microtubule assembly dynamics and cancer cell proliferation. Biochemistry. 2006;45:5440–5449.

[29] Skiles JW, Gonnella NC, Jeng AY. The design, structure, and clinical update of small molecular weight matrix metalloproteinase inhibitors. Curr Med Chem. 2004;11:2911–2977.

[30] Nielsen FE, Jacobsen P, Worsaae A, Arkhammar POG, Wahl P, Hansen JB. 2-(4-Methoxyphenoxy)-5-nitro-N-(4-sulfamoylphenyl)benzamide activates Kir6.2/SUR1 K_{ATP} channels. Bioorg & Med Chem Lett. 2004;14:5727–5730.

[31] Siwach K, Kumar A, Panchal H, Kumar R, Bhardwaj JK, Angeli A, Supuran CT, Sharma PK. Selective inhibition of carbonic anhydrase IX by sulphonylated 1,2,3-triazole incorporated benzenesulphonamides capable of inducing apoptosis. J Enzyme Inhib Med Chem. 2022;37:1454-1463.

[32] Bonardi A, Nocentini A, Bua S, Combs J, Lomelino C, Andring J, Lucarini L, Sgambellone S, Masini E, McKenna R, Gratteri P, Supuran CT. Sulfonamide Inhibitors of Human Carbonic Anhydrases Designed through a Three-Tails Approach: Improving Ligand/Isoform Matching and Selectivity of Action. J Med Chem. 2020;63:7422-7444.

[33] Krymov SK, Scherbakov AM, Dezhenkova LG, Salnikova DI, Solov'eva SE, Sorokin DV, Vullo D, De Luca V, Capasso C, Supuran CT, et al. Indoline-5-Sulfonamides: A Role of the Core in Inhibition of Cancer-Related Carbonic Anhydrases, Antiproliferative Activity and Circumventing of Multidrug Resistance. Pharmaceuticals. 2022;15:1453.

[34] Moi D, Deplano A, Angeli A, Balboni G, Supuran CT, Onnis V. Synthesis of Sulfonamides Incorporating Piperidinyl-Hydrazidoureido and Piperidinyl-Hydrazidothioureido Moieties and Their Carbonic Anhydrase I, II, IX and XII Inhibitory Activity. Molecules. 2022;27:5370.

[35] Vullo D, Luca VD, Scozzafava A, Carginale V, Rossi M, Supuran CT, Capasso C. The extremo-α-carbonic anhydrase from the thermophilic bacterium Sulfurihydrogenibium azorense is highly inhibited by sulfonamides. Bioorg Med Chem 2013;21:4521–4525.

[36] Kim DK, Lee JY, Lee N, Ryu DH, Kim JS, Lee S, Choi JY, Ryu JH, Kim NH, Im GJ, Choi WS, Kim TK. Synthesis and phosphodiesterase inhibitory activity of new sildenafil analogues containing a carboxylic acid group in the 5'-sulfonamide moiety of a phenyl ring. Bioorg Med Chem. 2001;9:3013–3021.

[37] Natarajan A, Guo Y, Harbinski F, Fan YH, Chen H, Luus L, Diercks J, Aktas H, Chorev M, Halperin JA. Novel arylsulfoanilide-oxindole hybrid as an anticancer agent that inhibits translation initiation. J Med Chem. 2004;47:4979–4982.

[38] Carta F, Scozzafava A, Supuran CT. Sulfonamides: a patent review (2008-2012). Expert Opin Ther Pat. 2012;22:747–758.

[39] Bukowski RM, Yasothan U, Kirkpatrick P. Pazopanib. Nat Rev Drug Discovery. 2010;9:17–18.

[40] Harvard C, Sharpe AH, Butte MJ, et al. Inventor; Harvard University, Inc., Assignee. Modulators of Immunoinhibitory Receptor PD-1, and Methods of Use Thereof: United States Patent US 2011020046. 2011 Jul 07.

[41] Sharpe AH, Pauken KE. The diverse functions of the PD1 inhibitory pathway. Nat Rev Immunol. 2018;18:153-167.

[42] Galal AMF, Soltan MM, Ahmed ER, Hanna AG. Synthesis and biological evaluation of novel 5-chloro-N-(4-sulfamoylbenzyl) salicylamide derivatives as tubulin polymerization inhibitors. MedChemComm 2018;9:1511.

[43] Galal AMF, Fayad W, Mettwally WSA, Gomaa SK, Ahmed ER, El-Refai HA, Hanna AG. Cytotoxicity of multicellular cancer spheroids, antibacterial, and antifungal of selected sulfonamide derivatives coupled with a salicylamide and/or anisamide scaffold. Med Chem Res 2019;28:1425-1440.

[44] Galal AMF, Mohamed HS, Abdel-Aziz MM, Hanna AG. Development synthesis, and biological evaluation of sulfonyl-α-l-amino acids as potential anti-Helicobacter pylori and IMPDH inhibitors. Arch Pharm (Weinheim). 2021;354(6):e2000385.

[45] Galal AMF, DiaaAtta, Abouelsayed A, Ibrahim MA, Hanna AG. Configuration and molecular structure of 5-chloro-N-(4-sulfamoylbenzyl) salicylamide derivatives. Spectrochim Acta A Mol Biomol Spectrosc. 2019;214:476–486.

[46] Galal AMF, Mahmoud K. Antiproliferative Evaluation and Molecular Docking studies of some Sulfonyl-α-L-amino acid Derivatives coupled with Anisamide Scaffold. Egypt J Chem. 2021;64:3465-3474.

[47] Galal AMF, Shalaby EM, Abouelsayed A, Ibrahim MA, Al-Ashkar E, Hanna AG. Structure and absolute configuration of some 5-chloro-2-methoxy-N-phenylbenzamide derivatives. Spectrochim Acta Part A. 2018;188:213–221.

[48] Abdelaziz AM, Yu M, Li P, Zhong L, Singab AB, Hanna AG, Abouzid KA, Mekhael MKG, Wang S. Synthesis and Evaluation of 5-Chloro-2-Methoxy-N-(4-Sulphamoylphenyl) Benzamide Derivatives as Anti-cancer Agents. Med chem 2015;5(5):253-260.

[49] Trott O, Olson AJ. AutoDock Vina: Improving the speed and accuracy of docking with a new scoring function, efficient optimization, and multithreading. J Comput Chem. 2010;31:455–461.

[50] Lee DY, Im E, Yoon D, Lee YS, Kim GS, Kim D, Kim SH. Pivotal role of PD-1/PD-L1 immune checkpoints in immune escape and cancer

progression: Their interplay with platelets and FOXP3+Tregs related molecules, clinical implications and combinational potential with phytochemicals. Semin Cancer Biol. 2022;86:1033-1057.

[51] Alimirah F, Chen J, Basrawala Z, Xin H, Choubey D. DU-145 and PC-3 human prostate cancer cell lines express androgen receptor: implications for the androgen receptor functions and regulation. FEBS Lett. 2006;580(9):2294-300.

[52] Tai S, Sun Y, Squires JM, Zhang H, Oh WK, Liang CZ, Huang J. PC_3 is a cell line characteristic of prostatic small cell carcinoma. Prostate. 2011;71(15):1668-79.

[53] Johnston ST, Shah ET, Chopin LK, Sean McElwain DL, Simpson MJ. Estimating cell diffusivity and cell proliferation rate by interpreting IncuCyte ZOOM™ assay data using the Fisher-Kolmogorov model. BMC Syst Biol. 2015;9:38.

[54] Villegas J, McPhaul M. Establishment and culture of human skin fibroblasts. Curr Protoc Mol Biol. 2005;71(1):28.3.1-28.3.9. https://doi.org/10.1002/0471142727.mb2803s71

[55] Cheng F, Li W, Zhou Y, Shen J, Wu Z, Liu G, Lee PW, Tang Y. admetSAR: a comprehensive source and free tool for assessment of chemical ADMET properties. J Chem Inf Model. 2012;52(11):3099-105.